12-2010

Dynamic Remodeling of the Stressed Heart: Role of Protein Degradation Pathways

Deborah Vela

DYNAMIC REMODELING OF THE STRESSED HEART: ROLE OF PROTEIN

DEGRADATION PATHWAYS

A

THESIS

Presented to the Faculty of

The University of Texas

Health Science Center at Houston

and

The University of Texas

M. D. Anderson Cancer Center

Graduate School of Biomedical Sciences

in Partial Fulfillment

of the Requirements

for the Degree of

MASTER OF SCIENCE

by

Deborah Vela, M.D.

Houston, Texas

December 2010

ACKNOWLEGEMENTS

I would like to first thank my advisor, Dr. Heinrich Taegtmeyer, for his support and guidance. Special thanks to Dr. Anil Reddy for his collaboration, expertise and assistance with the Doppler system; and to Dr. Mark Entman for his generosity. Thanks are also due to my mentor, Dr. Maximilian Buja for his understanding and support. Thanks to Ms. Patricia Sikes at Charles River Labs for helping us achieve the model needed for this study. Thanks to Ms. Roxy Tate for her diligence and willingness to help. Thanks to all the members of the Taegtmeyer lab for their support, camaraderie and providing a positive atmosphere, even during times of high stress.

Thanks to my Advisory Committee: Drs. Andreas Bergmann, Maximilian Buja, Diana Milewicz, Melvin Klegerman and Mark Entman.

Thanks to the GSBS, particularly Deans Victoria Knutson and Thomas Goka, for their continued efforts to make each student succeed.

Very special thanks to my family for providing endless support in all too many aspects.

DYNAMIC REMODELING OF THE STRESSED HEART: ROLE OF PROTEIN

DEGRADATION PATHWAYS

Publication No.:_____

Deborah Vela, M.D.

Supervisory Professor: Heinrich Taegtmeyer, M.D., DPhil

The heart is a remarkable organ. In order to maintain its function, it remodels in response to a variety of environmental stresses, including pressure overload, volume overload, mechanical or pharmacological unloading and hormonal or metabolic disturbances. All these responses are linked to the inherent capacity of the heart to rebuild itself. Particularly, cardiac pressure overload activates signaling pathways of both protein synthesis and degradation. While much is known about regulators of protein synthesis, little is known about regulators of protein degradation in hypertrophy. The ubiquitin-proteasome system (UPS) selectively degrades unused and abnormal intracellular proteins. I speculated that the UPS may play an important role in both qualitative and quantitative changes in the composition of heart muscle during hypertrophic remodeling. My study hypothesized that cardiac remodeling in response to hypertrophic stimuli is a dynamic process that requires activation of highly regulated mechanisms of protein degradation as much as it requires protein synthesis. My first aim was to adopt a model of left ventricular hypertrophy and determine its gene expression and structural changes. Male Sprague-Dawley rats were submitted to ascending aortic banding and sacrificed at 7 and 14 days after surgery. Sham operated animals served as controls. Effective aortic banding was confirmed by hemodynamic assessment by Doppler flow measurements *in vivo*. Banded rats showed a four-fold increase in peak stenotic jet velocities. Histomorphometric analysis revealed a significant increase in myocyte size as well as fibrosis in the banded

animals. Transcript analysis showed that banded animals had reverted to the fetal gene program. My second aim was to assess if the UPS is increased and transcriptionally regulated in hypertrophic left ventricular remodeling. Protein extracts from the left ventricles of the banded and control animals were used to perform an *in vitro* peptidase assay to assess the overall catalytic activity of the UPS. The results showed no difference between hypertrophied and control animals. Transcript analysis revealed decreases in transcript levels of candidate UPS genes in the hypertrophied hearts at 7 days post-banding but not at 14 days. However, protein expression analysis showed no difference at either time point compared to controls. These findings indicate that elements of the UPS are downregulated in the early phase of hypertrophic remodeling and normalizes in a later phase. The results provide evidence in support of a dynamic transcriptional regulation of a major pathway of intracellular protein degradation in the heart. The discrepancy between transcript levels on the one hand and protein levels on the other hand supports post-transcriptional regulation of the UPS pathway in the hypertrophied heart. The exact mechanisms and the functional consequences remain to be elucidated.

TABLE OF CONTENTS

LIST OF ILLUSTRATIONS

ix

LIST OF TABLES

ABBREVIATIONS

4EBP1	Eukaryotic initiation factor-4E (eIF-4E) binding protein 1
Akt	Protein kinase B
ANF	Atrial natriuretic factor
FoxO	Forkhead box subfamily O
GAPDH	Glyceraldehyde 3-phosphate dehydrogenase
GLUT1	Glucose transporter 1
GLUT4	Glucose transporter 4
GSK-3 β	Glycogen synthasekKinase-3ß
LV	Left ventricle
MCD	Malonyl-CoA decarboxylase
mCPT-I	Muscle carnitine palmitoyl transferase I
mGS	Muscle glycogen synthase
MHC-α	Myosin heavy chain alpha
MHC-β	Myosin heavy chain beta
mTOR	Mammalian target of rapamycin
MAFbx	Muscle atrophy F-box
MuRF1	Muscle ring finger-1
p70S6K	P70 ribosomal S6 kinase
PCR	Polymerase chain reaction
PDK2	Pyruvate dehydrogenase kinase 2
PDK4	Pyruvate dehydrogenase kinase 4

PPAR-α	Peroxisome proliferator activated receptor alpha
RAAB	Rats whose ascending aorta was banded
RNA	Ribonucleic acid
UCP2	Uncoupling protein 2
UCP3	Uncoupling protein 3
UPS	Ubiquitin proteasome system

Footnote: Please note that multiple references appear in alphabetical order and not in chronological order.

Chapter 1: INTRODUCTION

The rapid implementation of new scientific methodologies over the last 30 years has resulted in a wide acceptance for the concept of "the dynamic state of the body constituents" (Schoenheimer 1942). In this regard, the heart is no exception to all organs of the mammalian organism (Waterlow and others 1978). Indeed, a recent review by Hill and Olson (Hill and Olson 2008) stresses the point that the heart remodels in response to a large variety of environmental stimuli. These include pressure overload, volume overload, mechanical or pharmacological unloading, prolonged inotropic stimulation, and hormonal or metabolic disturbances (e.g. diabetes mellitus, or thyroid dysfunction). All these responses are linked to the heart muscle cell's capacity to rebuild itself. Particularly, cardiac pressure overload activates signaling pathways of both protein synthesis and degradation.

Much is known about signaling pathways of hypertrophy, but little is known about regulators of protein degradation in this same setting. Based on preliminary data from our lab, we speculated that both qualitative and quantitative changes in the composition of heart muscle cells are the result of highly regulated mechanisms of protein degradation (Razeghi and others 2006a; Razeghi and others 2006b; Razeghi and Taegtmeyer 2006). The ubiquitin-proteasome system (UPS) is the major proteolytic system within the cell, in charge of the selective degradation of unused and abnormal proteins. Thus, in this context the (UPS) may turn out to be a major player in cardiac remodeling.

The concept of protein turnover in the heart cannot be fully grasped without some basic knowledge regarding the heart's structure and constituents. Approximately 70% to 75% of the heart is composed of contractile muscle cells, the cardiomyocytes (Opie 2004). Each cardiomyocyte is filled with functional organelles and bundles of contractile units called sarcomeres.

These sarcomeres are the smallest cardiac muscle contractile units of the heart, thus cardiac performance is reliant on their construction and turnover. They are a constantly changing structure, assembled and degraded as evidenced by the half life of their major components, depicted in **Table 1**. This dynamic turnover of the structural proteins (**Figure 1**) of the sarcomere constitutes a continuous remodeling that allows adaptation to stressors (Willis and others 2009). However, despite the significance of this vital component of cardiac function, knowledge of the actual mechanisms responsible for its turnover is rudimentary (Razeghi and Taegtmeyer 2006).

Table 1. Half life of sarcomeric proteins

	$t_{1/2}$
Actin	7-10 days
Myosin	5-8 days
Troponin (T/I/C)	3-5 days
Tropomyosin	7-10 days
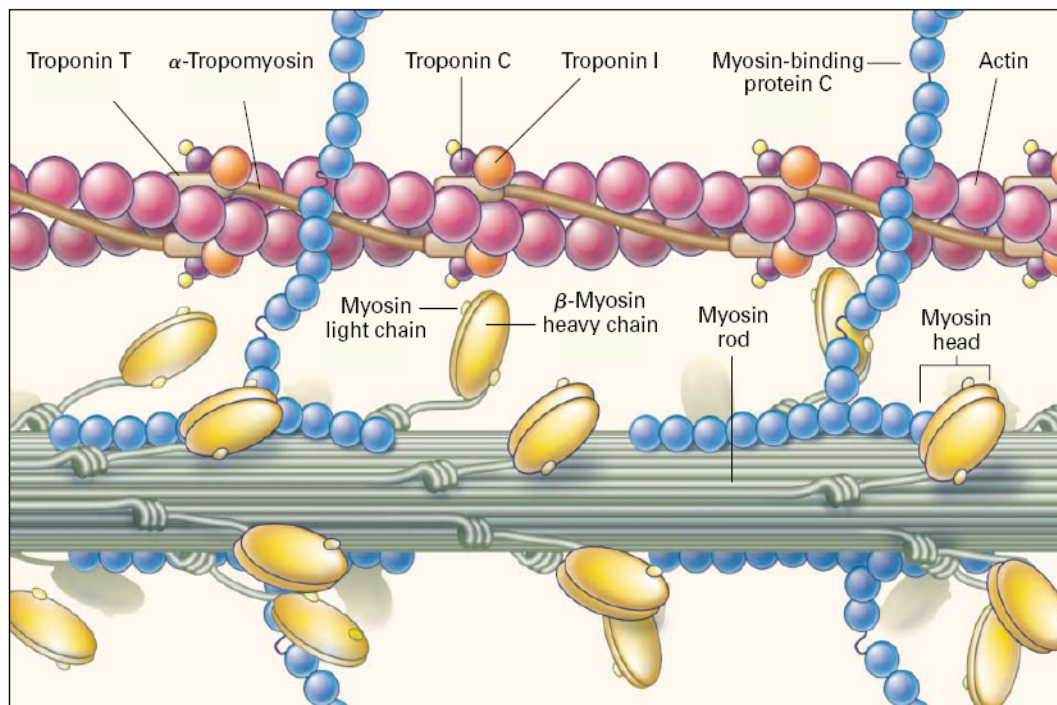
Figure 1. Components of the sarcomere. Apapted with permission from *New England Journal of Medicine* (Spirito and others 1997).

Chapter 2: HYPERTROPHIC REMODELING OF THE

STRESSED HEART

The notion of the dynamic state of body constituents discussed in the previous section can be nicely illustrated in the heart's remarkable plasticity (**Figure 2**). In conditions of either physiological or disease states, the heart can increase its mass up to 60% (Depre and others 1998; Fagard 2003; Hill and Olson 2008; Milliken and others 1988; Rockman and others 1991). Conversely, the heart can decrease its mass up to 50% during unloading (Depre and others 1998; Hill and Olson 2008; Sharma and others 2006).

When biomechanical stress increases, cardiomyocyte hypertrophy results. By definition hypertrophy is indicated by greater orderliness of the sarcomere, increased rates of protein synthesis, and enlarged cardiomyocytes. Additionally, the cellular phenotype alterations come after, and are concurrent with, the reinduction of the fetal gene program, which will be discussed below (Depre and others 1998; Frey and Olson 2003; Rajabi and others 2007; Taegtmeyer and others 2010).

The cellular changes that occur in hypertrophy eventually result in an increase in left ventricular wall thickness. This phenomenon can be explained by Laplace's law, where amplified thickness of the left ventricular wall decreases wall stress, and thus reduces oxygen expenditure. In this view, the onset of cardiac hypertrophy may be a *adaptive* response (Morisco and others 2003). However, though hypertrophy might at some point result in normal wall tension, there is an association with detrimental results such as sudden death or advancement towards explicit heart failure when the hypertrophic stimulus is sustained. Left ventricular diastolic and systolic dysfunction, with ensuing progress towards congestive heart failure, begins with cardiac hypertrophic remodeling. This raises the thought that impairing this compensatory response might result in progression from cardiac hypertrophy to left ventricular dysfunction and eventually heart failure and death (Morisco and others 2003). At this stage, the hypertrophic response is considered *maladaptive*.
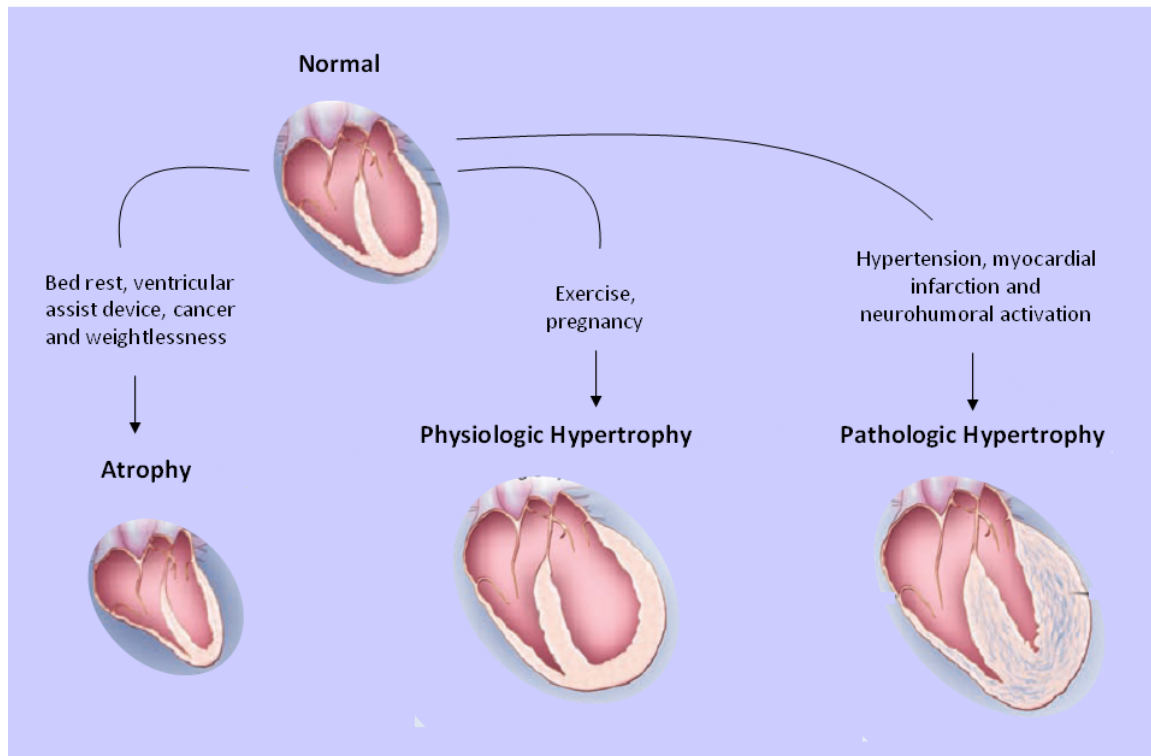
Figure 2. The heart displays a broad dynamic range in its adaptation of mass and size in response to the physiologic environment. This is evidenced by its capacity to undergo hypertrophy or atrophy in response to physiological and pathological demands. Adapted with permission from the *New England Journal of Medicine* (Hill and Olson 2008).

From a structural standpoint, cardiac hypertrophy has been divided into *concentric* vs. *eccentric*. Concentric hypertrophic remodeling is typified by increased thickness of the cardiomyocyte, generally in response to pressure overload. On the other hand, eccentric hypertrophy results in greater myocyte length, generally considered in response to a volume overload. In addition, hypertrophy has also been classified as *physiological* vs. *pathological* depending on whether it progresses or not to a disease state. Physiological hypertrophy is considered in general as being a favorable adaptation that does not cause or contribute to disease (Buttrick and Scheuer 1987). Moreover, genetic studies that compare physiological (exercise-induced) vs. pathological hypertrophy (hypertension), in small animal models, have described unique gene expression patterns between these two types (Iemitsu and others 2001; Kong and others 2005; Strom and others 2005). Noticeably, physiological hypertrophy does not induce the fetal gene program (*discussed below*).

2.1 <u>Rat Models of Cardiac Hypertrophy</u>

While no single animal model can reproduce human disease, they contribute to our understanding of cardiovascular disease by allowing us to evaluate particular aspects of disease processes such as pathogenesis and signaling pathway mechanisms. In this regard the rat carries several advantages such as economical convenience, the ability to replicate cardiovascular syndromes in a fairly comparable manner to human. In addition, it allows hemodynamic assessment and surgical interventions with greater ease than in mice (Doggrell and Brown 1998).

The main objective in producing an animal model of left ventricular hypertrophy (LVH) is to be able to generate a pressure gradient to stress the left ventricle in a manner similar to what is observed in a patient with increased afterload. Afterload is the result of

Table 2. Common rat models of left ventricular hypertrophy.

Model	Comment	References
Exercise-induced LVH	Treadmill, swimming or resistance training. Duration and intensity of the protocols vary depending on the study goal.	Arcos and others 1968, Flaim 1980, Tamanaki and others 1992
Pressure overload (aortic banding) Ascending aortic banding Transverse aortic banding Abdominal aortic banding	Partial constriction of the aorta produces a rapid model generally exclusive for LV hypertrophy (and not failure) in a short time. The constriction site and percent occlusion can influences the speed at which the hypertrophy develops. Ascending placement usually produces most rapid results and abdominal placement, the slowest. This model has been used to define structural changes and signalling pathways that develop during hypertrophy, but the short, sudden pressure overload does not mimic most disease states in humans.	Cutilletta and others 1975, Mercadier and others 1981, Klienman and others 1978
Renal artery occlusion	One-kidney, one-clip (1K1C) or two-kidney, two-clip (2K2C) produce a sudden volume overload hypertension which induces concentric LV hypertrophy, fibrosis and finally heart failure.	Goldblatt and others 1934
Pharmacological	Catecholamines (noradrenaline and isoprenaline). Noradrenaline leads to selective LV hypertrophy. Isoprenaline produces myocardial necrosis and progressive LV enlargement.	Brown and others 1992, Mende and others 1992
Spontaneously hypertensive rats (SHR)	Outbred from Wistar male with spontaneous hypertension. Pre-hypertensive for first 6-8 weeks. Hypertension (100-120 mmHg systolic) develops over next 12-14 weeks. Produces stable, chronic disease with predictable symptoms. Develops heart failure by ~1.5 years of age.	Kurtz and Morris 1987, Adams and others 1989
Dahl/Rapp salt sensitive rats	The development of hypertension and heart failure can be controlled by the amount of salt in their diet. Addition of 8% salt at 6 weeks of age leads to concentric LVH by 11 weeks and marked LV dilatation by 15-20 weeks.	Dahl and others 1975
Transgenics	TGR(mREN2)27 - transgenic rat that harbors the murine Ren-2 gene and exhibits hypertension.	Lee and others 1996

the ventricles contracting against pressure in order to expel ejected blood. In the context of

greater afterload, the left ventricle has to produce greater pressure to release the aortic valve

for ejecting blood into the systemic circulation. When this occurs, it is characterized as

pressure overload, and is common in systemically hypertensive patients or in those patients

with aortic stenosis. The chart presented as **Table 2** summarizes the most common rat

models utilized for the induction of LVH. It is worth noting that, because sustained pressure

overload will, in due course, result in heart failure, almost all of the models listed below

eventually develop a failing heart and are often also used as a model for this condition. The

length of time before LVH progresses to heart failure can be loosely predetermined in each

model. However, in some models, such as those that involve aortic banding, the degree and

location the of aortic constriction can significantly affect the time course of the LVH before

it results in failure. This eventual shift in all models from compensated LVH to heart failure

highlights the importance of the concept of the dynamic nature of the heart's adaptation to

stimuli, as pointed out in our introductory chapter and in the previous sections of the current

chapter. The laboratory's previous experience was with banding of the ascending aorta in

the rat (Depre and others 1998; Doenst and others 2001; Young and others 2001a; Young

and others 2001b).

2.2 Isoforms in the Heart and the Fetal Gene Program

During conditions of stress, the heart reverts to a gene expression pattern that is

similar to that seen during fetal life. The ultimate goal of this gene expression reversion

appears to be the maintenance of cardiac efficiency and cell survival under stress. This is

attained through the reactivation of developmental transcription factors and a series of

isoform switches in genes that encode for both contractile and structural proteins, as well as

genes of energy substrate metabolism. These changes shift the heart to a more energy efficient state to endure stress and are collectively known as the ''fetal gene program''. This gene expression pattern is prevalent in many pathophysiologic scenarios such as hypoxia, ischemia, hypertrophy and atrophy, all of which display vast remodeling and a decreased pace of the cardiomyocyte aerobic metabolism (Rajabi and others 2007; Taegtmeyer and others 2010).

A list of the isoform switches that have been observed in the rat heart is shown in **Table 3** taken from (Rajabi and others 2007). See also (Depre and others 1998; Izumo and others 1987; Izumo and others 1988; Mercadier and others 1981; Schwartz and others 1986) However, for the purposes of this study, I will focus of the contractile proteins of the heart relevant for our study.

Myosin heavy chains. The myosin molecule consists of 2 MHCs, 2 myosin alkali light chains (MLC) and 2 regulatory myosin light chains (MLC2). There are 2 isoforms that make up the heavy-chain subunits that house the location for ATPase activity, α and β, both having a presence in the ventricles and atria. These isoforms are manufactured by 2 unique isogenes that are located next to one another on the same chromosome: the β gene is located 4,000 nucleotides "upstream" of the α -gene. The simultaneous presence of two heavy chain and four light-chain forms might the formation of many different myosin isozymes if all combinations of heavy and light chains were possible. However, so far, three different myosin isozymes have been characterized in mammalian ventricular muscle V1, V2, and V3. Isozymes V1, and V3 are composed of $\alpha\alpha$- and $\beta\beta$-homodimers, respectively, whereas V2 is an $\alpha\beta$-heterodimer. (Schwartz and others 1992)

β-MHC is generated in accompaniment to hemodynamic (pressure) or metabolic stress. The degree to which the isoform changes depends on the preliminary phenotype. The preliminary low percentage of β-MHC (O-10%) in rat ventricular muscle provides for potentially large increases. β-MHC can reach as high as 80% of all of the myosin in hypertrophied rat ventricles, and its percentage is linked to the amount of hypertrophy. This shift is, nonetheless, reversible. (Schwartz and others 1992)

Table 3. Transcriptional changes in the rodent heart.

	Adult	Fetal	Hypertrophy
ANF	=	=	↑
MHC-α	↑	↓	↓
MHC-β	↓	↑	↑
Cardiac α-actin	↑	↓	↓
Skeletal α-actin	↓	↑	↑
GLUT1	=	=	=
GLUT4	↑	↓	↓
mCPT-I	↑	↓	↓
ICPT-I	=	=	=
mCK	↑	↓	↓
PPAR-α	↑	↓	↓
PDK2	↑	↓	↓
PDK4	↑	↓	↓
mGS	↑	↓	↓
MCD	↑	↓	↓
UCP2	↑	↓	↓
UCP3	↑	↓	↓

Adapted from (Rajabi and others 2007)

Chapter 3: PROTEIN TURNOVER IN THE HEART

Most of what we know so far regarding the proteolytic systems that may operate in the heart is derived from studies in skeletal muscle (Mitch and Goldberg 1996). To date, the most relevant proteolytic systems known in the heart are: a) the calpain system, b) the UPS, c) autophagy (**Figure 3**). After a brief description of the systems of protein degradation, I will focus on the UPS due to its newly acknowledged and emerging role in cardiac disease.
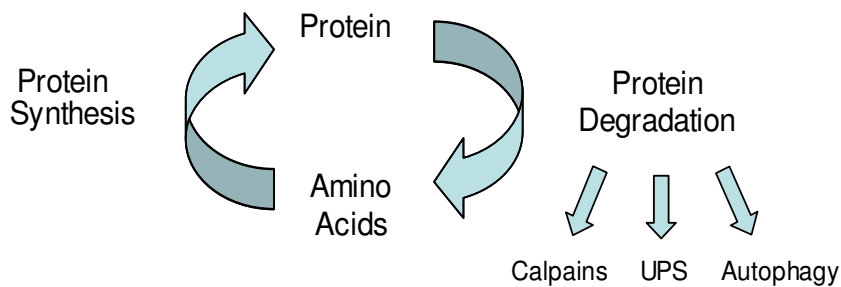
Figure 3. Dynamic relationship of protein synthesis and degradation.

2.2 <u>The calpain system</u>

Calpains are clusters of non-lysosomal cysteine proteases, dependent on calcium, that are expressed in every cell (Razeghi and Taegtmeyer 2006; Willis and others 2009). The calpain system is present in the heart, where it has been implicated in ischemia reperfusion-induced injury (Singh and others 2004). Calpains break up myofibrillar proteins and render them accessible by the UPS (Goll and others 2003; Razeghi and Taegtmeyer 2006). Calpain 1 can be found closely associated with myofibrils of skeletal muscle, bound snugly to the large protein titin in a calcium-dependent fashion. Recent discoveries show that calpain-1 is required for mediation of sarcomeric protein dissociation from the assembled myofibril to

allow subsequent degradation by the UPS system (Raynaud and others 2005; Willis and others 2009).

2.4 The Ubiquitin-Proteasome System

History. Proteolytic activity that is ATP-dependent was first detected during the 1970s (Goll and others 1989), but the workings of the molecules behind this activity only emerged in the early 1990s (Bochtler et al., 1999; Glickman and Cienchanover, 2002; Cienchanover, 2005). It quickly was observed that the relationship of the proteasome to intracellular protein turnover is like the link between the ribosome and intracellular protein synthesis. Since then, there has been intense pursuit of the ubiquitin proteasome system, and the 2004 Nobel Prize in Chemistry was awarded to the discoverers of ubiquitin-mediated protein degradation, Avram Hersko, Aaron Cienchanover and Irwin Rose (Goldberg 2005; Goll and others 2008).

Today the UPS is recognized to play an integral role in various cellular processes, including the regulation of cell mass, oversight of protein quality and apoptosis (Wang and others 2008; Willis and Patterson 2006). Researchers such as David Glass in Boston and Cam Patterson in North Carolina have contributed to furthering the knowledge and role of the UPS, particularly in the fields of skeletal and cardiac muscle, respectively.

Structure and Function. There are two consecutive steps for degrading a protein through the ubiquitin/proteasome pathway: 1) multiple ubiquitin moieties and the substrate must be conjoined , and 2) the tagged protein must be degraded by the downstream 26S proteasome complex (**Figure 4**). These are carried out by subsequent actions of three enzyme types. First, ubiquitin is triggered by the ubiquitin-activating enzyme (E1) in a reaction that is
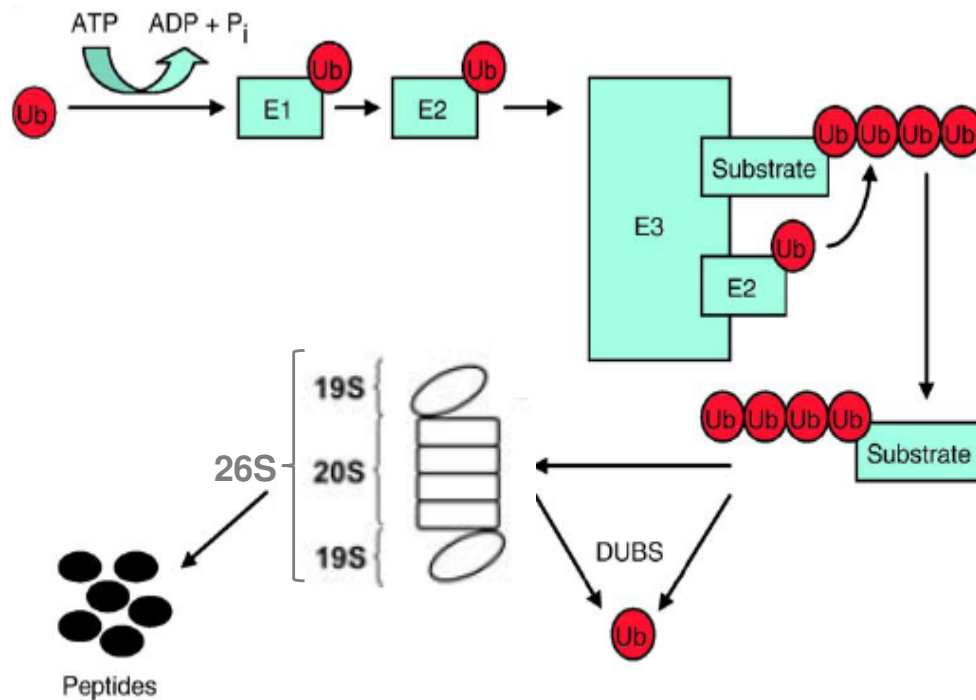
Figure 4. Scheme of the ubiquitin-proteasome system. Ubiquitination involves 3 steps: E1 activates ubiquitin in an ATP-dependent manner; an E2 enzyme transfers ubiquitin from E1; and an E3 enzyme facilitates the transfer of ubiquitin to a specific target protein substrate. Adapted, with permission from *Journal of Molecular and Cellular Cardiology* (Willis and Patterson 2006).

dependent on ATP. After this activation, the ubiquitin is transported to an ubiquitin-conjugating enzyme (E2), and from there joined to the lysine residue in proteins that are to be degraded. The ubiquitin ligases (E3) catalyze the reaction. Through repetition of these procedures, an ubiquitin chain is assembled. The ubiquitin-conjugated proteins are subsequently identified by the 19S subunit of the proteasome for degradation in 20S proteasome. The proteasome next releases the peptides, which are then degraded to amino acids by peptidases in the cytoplasm. The ubiquitin molecules are released for reuse, a process aided by ubiquitin recycling enzymes known as deubiquitinating enzymes (DUBs) (Glickman and Ciechanover 2002; Razeghi and Taegtmeyer 2005).

Ubiquitination. The 26S proteasome recognizes substrates joined to a poly-ubiquitin chain; however, it is noteworthy that ubiquitination has independently significant roles from that of the proteasome. These roles include monitoring of the activity of transcription factors, regulation of gene transcription and autophagy, and allowing the same target to be mono, multi and polyubiquitinated. When substrates are joined to a poly-ubiquitin chain through their Lysine 48, they are usually singled out for degradation by the proteasome. Nonetheless, ubiquitin is able to assemble ubiquitin chains via connections to other lysine residues. These are considered "non-canonical" forms of ubiquitination, such as in the case of ubiquitin chains joining to a substrate at Lysine residue Lys11, Lys29, or Lys63. This type of chain formation can be related to protein localization, DNA repair or cell signaling. When there is mono-ubiquitination of lysine residues, the outcome is generally modulation of DNA repair, transcription or histone modification. (Mearini and others 2008; Willis and Patterson 2006)

Ubiquitin ligases (E3) pertinent to cardiac hypertrophy: MAFbx and MuRF1. At first, these two ligases, muscle-atrophy F-box (MAFbx/Atrogin1) and muscle-specific ring finger-1 (MuRF1), detected only in skeletal muscle and cardiac tissue, were identified as essential players in skeletal muscle atrophy (Bodine and others 2001a). More recent studies have determined the role of these proteins in cardiac hypertrophy and confirmed their E3 ubiquitin ligase activity. To be specific, both of these ligases (MAFbx and MuRF1) are capable of inhibiting cardiac hypertrophy through their interaction with key elements of the hypertrophic signaling pathways (Willis and Patterson 2006).

Cardiac hypertrophy is limited by MAFbx/Atrogin1 via its effect on calcineurin. Calcineurin is a phosphatase which dephosphorylates NFAT (Molkentin and others 1998), culminating in the transcription of hypertrophy-associated genes. Atrogin1 rarefies this calcineurin-dependent activation of genes by interfering with NFAT translocation. This effect of MAFbx over calcineurin activity has been observed both in isolated cardiomyocytes and in mice with cardiac-specific Atrogin1 over-expression during the induction of pathologic cardiac hypertrophy (Glickman and Ciechanover 2002; Mearini and others 2008; Willis and Patterson 2006; Willis and others 2009).

The muscle ring finger-1 (MuRF1) protein has been associated with anti-hypertrophic effects through its ability to weaken PKCε activity and translocation (Ayra and others 2004). Prevention of cell signaling through PKCε subsequently inhibits focal adhesion formation, and will eventually impact the downstream ERK1/2 signaling (Glickman and Ciechanover 2002; Mearini and others 2008; Willis and Patterson 2006; Willis and others 2009). Additionally, MuRF1 has been shown to have a role in both protein quality control and the targeting of various sarcomeric components for degradation by the proteasome. These sarcomeric proteins include cardiac troponin I, C and T, myosin light

chain 2 (Kedar and others 2004), and titin. The fact that these sarcomeric components play a critical role in myocardial contractility suggests that MuRF1 could also play an important role in the normal physiology of the heart, separate from its role associated with hypertrophic remolding (Willis and Patterson 2006). Recent work also suggests that MuRF1 may play a role in the heart's energy metabolism through its interaction with several enzymes of ATP energy production in muscle (Witt and others 2005).

The Proteasome. The proteasome is not common or essential in bacteria, because of a differing ATP-dependent proteolytic system; it is frequent but not essential in archaea; and it is omnipresent and essential in eukaryotes, where it engages in the degradation of muscle protein. The proteasome (**Figure** 5) was discovered by Etlinger and Goldberg as part of a soluble ATP-dependent proteolytic system in 1977 (Etlinger and Goldberg 1977). It contains 2 structures: a 20S core particle that has a 19S complex bound to it and regulating its activity (the S signifies the sedimentation coefficient for each particle); together they form the 26S proteasome). The 20S core particle is composed of a barrel-like 700-kDa complex,15 nm high and 11 nm in diameter. In eukaryotic cells the particle contains 28 distinctive subunits composed of 2 classes: *α* and *β* subunits (each containing 14 of the 28 distinctive subunits). Each class has 7 unique gene products all of which are cloned and sequenced, and which vary in size from 20 to 35 kDa. The individual *α* subunits are homologous in sequence with one another, as are the individual *β* subunits homologous within themselves. However, they are not homologous in sequence with any other proteolytic enzyme. The proteolytic 20S particle is arranged in a total of 4 rings, each consisting of 7 subunits each. The *α* subunits make up the 2 outer rings, while the *β* subunits make up the 2 inner rings. The proteasome's proteolytic activity is the exclusive domain of the *β* subunits; the only functional catalytic

sites are the $\beta1$, $\beta2$, and $\beta5$ subunits , therefore, only 6 catalytic sites are present in one 20S proteasome. (Glickman and Ciechanover 2002; Goll and others 2008; Mearini and others 2008; Schwartz and Ciechanover 2009; Willis and Patterson 2006).

The barrel-like proteasome, as demonstrated by electron micrographs, has a central cavity while the crystallographic structure shows the location of all 6 catalytic sites to be inside the central cavity (Gray and others 1994; Lowe and others 1995; Unno and others 2002). The proteins composing the 19S regulatory particle guard the central cavity, resulting in a restricted opening to the central cavity of only 1.2 to 1.5 nm in diameter. This prevents protein molecules from entering the catalytic chamber if they have not first been unfolded. Accessability of the central cavity is the ultimate control of proteasome activity (Goll and others 2008).

Functions of the 19S regulatory subunit include polypeptide unfolding and substrate recognition. This regulatory subunit along with the 20S forms the 26S proteasome, a particle of 2,500-kDa which is highly unstable, resulting in a tendency to dissociate into subunits, including the 20S particle and others. The 19S regulatory complex is composed of a lid and a base **(Figure 5)**. The lid has 8 different polypeptides acting to bind and remove polyubiquitin chains from the polypeptide that is to be degraded for recycling. The base holds 6 homologous ATPases and 3 polypeptides (which are not ATPases). As the polypeptide enters the proteasom chamber, it is unfolded by the ATPases, which use the energy of ATP to accomplish this function; these enzymes can also be used in substrate binding. ATP hydrolysis is necessary for the attachment of ubiquitin to the fated polypeptide, resulting in a high energy requirement for protein degradation as regulated by the proteasome pathway. As many as 300 to 400 molecules of ATP are estimated to be
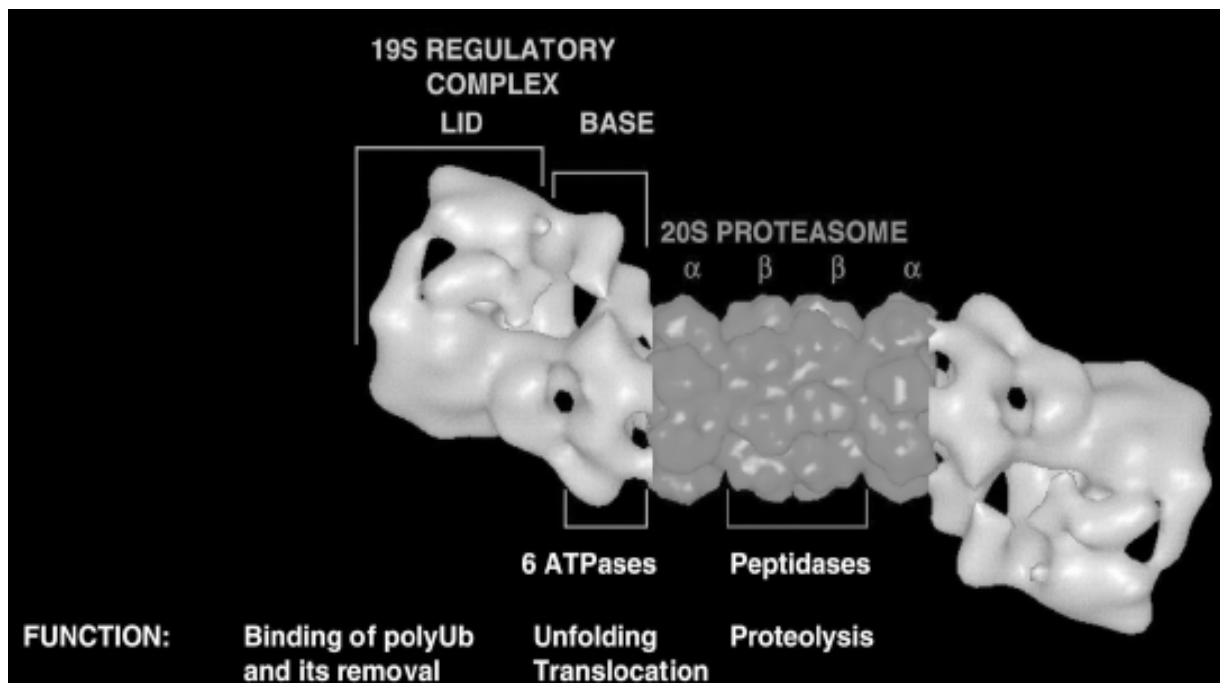
Figure 5. Electron tomography of the 26S proteasome and its components. Adapted, with permission, from The Journal of Animal Science (Goll and others 2008).

necessary for degradation of a protein by the proteasome (Glickman and Ciechanover 2002; Goll and others 2008; Mearini and others 2008; Schwartz and Ciechanover 2009; Willis and Patterson 2006). The regulatory particle can associate with one and/or the other end of the 20S proteasome, though the 20S particle can also remain a free particle (Voges and others 1999).

2.3 Autophagy

"*The interest in lysosomes as agents of endogenous proteolysis goes back to their discovery by de Duve in 1953* (De Duve and others 1953) *because they are the only cell organelles with substrate proteolytic capacity* (Dean and Barrett 1976) *and a known mechanism (autophagy) for acquisition of cellular material for degradation.*" (Wildenthal 1980)

Autophagy is a lysosome-based, highly conserved, cellular process in which long-lived proteins and organelles are degraded in the cell. (Cao and others 2009; Gustafsson and Gottlieb 2008; Mizushima 2004) One of its main functions is to provide nutrients to the cell during periods of starvation or nutrient-depletion. However, autophagy also has a role in the processing and elimination of misfolded proteins and turnover of organelles. Some authors further make the distinction between three subtypes of autophagy, mainly macroautophagy, microautophagy and chaperone-mediated autophagy. Nonetheless, due to being the most understood process of the three, macroautophagy and autophagy tend to be used synonymously in the literature. (Cao and others 2009; Gustafsson and Gottlieb 2008; Levine and Kroemer 2008; Mizushima 2004)

mTOR is among the key overseers of autophagy, where it functions as the major inhibitory signal that blocks autophagy in the presence of growth factors and abundant

nutrients. mTOR is linked to receptor tyrosine kinases by the PI3K/Akt signaling axis, with the result of suppression of autophagy response to insulin-like and other growth factors. (Levine and Kroemer 2008) Starvation, on the other hand, is a strong initiator of autophagy. This stimulus activates class III phosphatidylinositide-3-kinase (PI3K), which forms a complex with the rate-limiting autophagy protein, Beclin 1. This process then triggers autophagosome construction by bringing other autophagy proteins to the pre-autophagosomal membranes to form an isolation membrane. Other autophagy-related genes (ATG), such as ATG5, ATG12, and ATG16 aid in the development of the phagophore to surround the cytoplasmic contents. The phagophore edges then fuse, producing a double membrane structure called an autophagosome, which in the end fuses with a lysosome and forms an autolysosome. Here the sequestered material is digested by lysosomal proteases. (Cao and others 2009)

In the heart, there is substantiation that autophagy can be either advantageous or disadvantageous depending on the setting and degree of activation. The basal autophagic "housekeeping" functions are positive and necessary, as evidenced by the deleterious consequences of their disruption as seen in lysosomal storage diseases. (Ruivo and others 2009) In the setting of hemodynamic stress, autophagy has been associated with a maladaptive repsonse. (Zhu and others 2007) Its role in ischemia/reperfusion, however, has been more controversial, where there are claims of cardioprotection (Hamacher-Brady and others 2006) , as well as detrimental effects, particularly in the reperfusion phase (Matsui and others 2007). Conversely, markers and mediators of autophagy are downregulated in the failing human heart following mechanical unloading (Kassiotis and others 2009).

Chapter 4: MATERIALS AND METHODS

4.1. Experimental protocol.

In a model of induced left ventricular pressure overload, we assessed the role of the ubiquitin-proteasome system and its transcriptional regulation. The model was a modification of aortic banding in the rat heart previously described (Kleinman and others 1978; Young and others 2001b) in our lab. Animals were sacrificed at two time points and the number of animals was distributed as shown in **Figure 6** below:
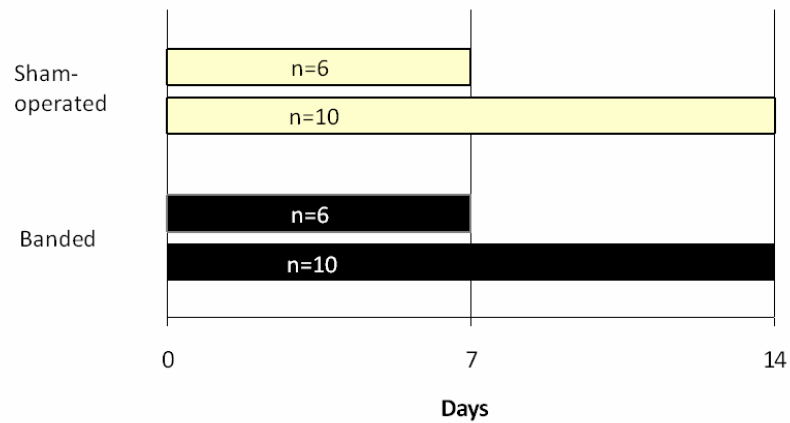
Figure 6. Diagram of the experimental design and time points.

From the total number of animals indicated above, a subset of animals was designated exclusively for histology:

o   7 days post-banding: 2 banded rats vs. 1 sham-operated rats

o   14 days post-banding: 2 banded rats vs. 1 sham-operated rats

4.2. Animals.

Male Sprague-Dawley rats, 175-200g, 6-7 weeks old, were purchased from Charles River Laboratories (Wilmington, MA).

4.3. Equipment.

ABI Prism® 7000 Sequence Detection System (Applied Biosystems, Carlsbad, CA); POLARstar OPTIMA fluorometer (BMG LABTECH, Cary, NC); MyCycler Thermal Cycler (#170-9701EDU, Bio-Rad, Hercules, CA); 20 MHz probe (20 MHz ultrasound pulsed Doppler and a computer-based Doppler signal processor, DSPW; Indus Instruments, Houston, TX).

4.4. Ascending aortic banding.

The surgery was performed at Charles River Laboratories (Wilmington, MA) by Dr. Amber Kang, Senior Surgical Specialist. The rats underwent ascending aortic banding to produce left ventricular hypertrophy (pressure overload)**.** Sham operated animals served as controls. The surgical technique is as follows: A ventral midline incision is made to expose the clavicle. The sternal manubrium is transected. The thymus gland is rostrally retracted to expose the aorta. The tissue around the aorta, between the brachiocephalic trunk and the heart, is isolated with forceps (**Figure 7**). A piece of 4-0 silk suture is passed around the aorta. A 21 gauge metal wire is positioned over the aorta and the silk suture is tied around both the aorta and the wire. The wire is then carefully removed under the ligature, leaving the aorta constricted to the O.D. of the wire. The air is expelled from the cavity of the mediastinum. The incision is closed with wound clips.

4.5. Hemodynamic Measurements.

This work was performed in collaboration with Dr. Anilkumar Reddy, Ph.D., in the laboratory of Dr. Mark Entman, in the Division of Cardiovascular Science, Baylor College of Medicine. Effective aortic banding was confirmed by hemodynamic assessment.

Figure 7. Location of aortic band placement.

Specifically, carotid and aortic arch blood flow velocities were measured by Doppler *in vivo* to assess the association of carotid blood flow velocity change to the degree of cardiac hypertrophy caused by ascending aortic banding. Doppler velocity signals of left and right carotid arteries were determined with a 20 MHz probe (20 MHz ultrasound pulsed Doppler and a computer-based Doppler signal processor, DSPW; Indus Instruments, Houston, TX) in animals 12 days post-surgery. The probe was positioned to the right and left of the neck, near the entrances to the carotid, angled toward the flow at 45°, to determine the flow velocity in the right and left carotid arteries. The pressure gradient (ΔP) across the stenosis was estimated using the simplified Bernoulli's equation ($\Delta P \approx 4V^2$) where V is the peak Doppler velocity measured at the stenotic orifice in the aorta (in banded rats) or aortic arch (in sham-operated rats). The aortic velocities were measured with a probe orientation such that the angle was close to 0°. These measurements were similar to the ones we made in mice (Li and others 2003a; Li and others 2003b). The measured Doppler signals were digitized, displayed, and stored using the DSPW system (Reddy and others 2005). As a rule, data was sampled in 2-second segments and then saved for subsequent analysis. During offline analysis peak velocities of aortic (V) and left (L) and right (R) carotid flow signals

were extracted. Left-to-right ratios (L/R) of flow velocities for each rat were also computed in order to limit rat-to-rat variations. Also, the average of L/R ratio for each group was computed. All parameter values are given as mean±SD (standard deviation).

4.6. Tissue Harvest.

At the defined time points, animals were sedated with pentobarbital. A thoracotomy was performed and the heart was excised, then freeze-clamped (while still beating) with aluminum tongues, cooled to the temperature of liquid nitrogen, as described by Wollenberger et al (ref 1960). Hearts designated for histology were fixed in formalin and later paraffin-embedded and sections were sliced at 5 microns thick. Sections were stained with H&E and Masson's trichrome stains.

4.7. RNA Extraction.

RNA extraction was carried out by conventional methods previously utilized in our laboratory (Chomczynski and Sacchi 2006). Snap frozen tissues from the left ventricles of sham-operated and RAAB were crushed by mortar and pestle until a thin powder was obtained. Liquid nitrogen was continuously added to prevent thawing. The powder obtained was transferred to a minimum of 1mL TRIZOL / 100mg tissue and mixed with a tissue homogenizer (Power Gen 35). Chloroform was added to the mixture for phase separation. After centrifugation, the top aqueous phase was transferred to a clean tube and isopropanol was added to produce RNA precipitation. After centrifugation, the RNA pellet was later washed with ethanol, allowed to air dry and finally re-suspended in approximately 80-100ul of DEPC water. RNA concentration was measured by spectrophotometry in a Nanodrop 1000 (Thermo Fisher Scientific, Wilmington, DE).

4.8. Quantitative Real-Time PCR Transcript Analysis.

The technique of real-time PCR (7700 Prism, Perkin-Elmer/ABI) is based on the hydrolysis of a particular fluorescent probe in every amplification cycle by the endonuclease activity of *Taq* polymerase (Heid and others 1996). Every PCR cycle shows increased fluorescent signalling in direct proportion to the number of probe molecules being hydrolyzed, itself an exact measure of the amount of template amplicons. The C_t (how many PCR cycles are necessary before the fluorescent signal reaches a detection threshold) is in direct proportion to the amount of input template enabling one to calculate, using a suitable standard, how many template molecules present themselves during the reaction. (Depre and others 1998)

mRNA transcript levels of all genes analyzed in this study were amplified using TaqMan® quantitative real-time reverse transcriptase PCR (qRT-PCR).(Latres and others 2005) The cDNA sequences were obtainable from NCBI's GenBank. (A list of the genes and their respective primers, probes and GenBank accesion numbers can be found in Table 1). PCR primers and fluorogenic probes were previously designed in our lab, from the corresponding cDNA sequences, using the Primer Express 2.0 software program (Applied Biosystems). Synthesis of oligos, probes and synthetic standards was performed by IDT (Latres and others 2005) The reverse transcription was performed with 60ng of total mRNA using Superscript II (Invitrogen), on a MyCycler Thermal Cycler (#170-9701EDU, Bio-Rad, Hercules, CA). Real-time PCR analysis was performed on an ABI prism 7000 (Applied Biosystems) instrument. The process involved denaturation at 95°C, then 40 cycles of denaturation at 95°C for 15 seconds, followed by annealing at 60°C for 1 minute. Absolute quantification of transcripts was based on known amounts of synthetic DNA standard. Each sample was run in triplicate, allowing evaluation of technical variability. For each sample, a

control lacking reverse transcription was incorporated, to clarify PCR amplification of contaminating genomic DNA. Total RNA concentration was used for normalization. All results are reported as copy number/total RNA. (Latres and others 2005; Satoh and others). **Table 4** lists primers and probes used in the experiments.

4.9. 20S Proteasome Activity Assay.

Protein extracts of tissue lysates from the left ventricles of banded and sham-operated animals were assayed with a CHEMICON® Proteasome Activity Assay Kit, as recommended by the manufacturer. This *in vitro* peptidase assay that uses the synthetic fluorogenic peptide LLVY-AMC as substrates to assess the overall catalytic activity of the UPS. It is based on the proteasome's capability to recognize LLVY. After cleavage from the labeled substrate LLVY-AMC, the fluorophore 7-Amino-4-methylcoumarin (AMC) is detected. A 380/460 nm filter set in a standard fluorometer can be used to quantify the free AMC fluorescence (Meng and others 1999).

4.10. Protein Extraction and Analysis.

Protein was extracted from pulverized frozen left ventricular tissue. The Bradford assay was used to determine the protein concentration of all samples (Pierce). Total protein homogenate samples (35µg) were denatured by 5 minutes of heating at 100°C, with subsequent separation by SDS-protein acrylamide gel electrophoresis (SDS-PAGE) and transfer to PVDF membranes (Bio-Rad, Cat.No. 162-0177). blocked with 5% (w/v) non-fat dried milk in TBS buffer containing 0.05% Tween-20 and then probed separately using primary antibodies. (A list of the primary antibodies employed by this study can be found in **Table 5**). Membranes were thoroughly washed and then incubated with horseradish–

Table 4. Primer and Probe Sequences Used in Real-Time Quantitative RT-PCR.

Gene		Sequence	GenBank #
ANF	Forward Reverse Probe	5'-AGTGCGGTGTCCAACACAG-3' 5'-CTTCATCGGTCTGCTCGCT-3' 5'-FAM-TCTGATGGATTTCAAGAACCTGCTAGACCAC-TAMRA	M27498
MHC-α	Forward Reverse Probe	5'-TGTGAAAAGATTAACCGGAGTTTAAG-3' 5'-TCTGACTTGCGGAGGTATCG-3' FAM-CCIAAGTCAGCCATCTGGGCACT-TAMRA	X15938
MHC-β	Forward Reverse Probe	5'-AAGTCCTCCCTCAAGCTCCTAAGT-3' 5'-TTGCTTTGCCTTTGCCC-3' FAM-CATCAGCICCAGCATAGTTGGCAAACA-TAMRA	X15939
MAFbx	Forward Reverse Probe	5'-GGCTGTTGGAGCTGATAGCA-3' 5'-GCTGGTCTTCAAGGACTTTCAGTAC-3' FAM-CACATCCCTGAGTGGCATCGA-TAMRA	AY059629
MuRF-1	Forward Reverse Probe	5'-ACAGCCACCAGGTGAAGG-3' 5'-GCAGCAGCTCACTCTTCTTCT-3' FAM-CTGAGCCACAAGTTTGACGCC-TAMRA	BC061824
PSMB4	Forward Reverse Probe	5'-GCGTAGCTTATGAAGCCCCTTCA-3' 5'-ACTCAGCACCGGTTGCTTCT-3' FAM'-TGGTGCATACTTGGCTCAGCC-TAMRA	NM031629

peroxidase-conjugated appropriate secondary antibodies. Levels of expression of each

protein were quantitated by densitometric analysis. Protein loading was normalized by

using monoclonal GAPDH antibody.(Kassiotis and others 2009; Zhang and others 2003)

4.11   Estimation of Cardiomyocyte Size.

Formalin-fixed, paraffin-embedded sections from the hearts of sham operated and

RAAB were stained with hematoxylin and eosin (H&E) and utilized for myocyte size

calculation. Digital images from the left ventricles of each heart were acquired with a bright

field microscope and a DP70 camera, at x400 magnification. The cross-sectional area of

individual myocytes was obtained by manual tracing and subsequent quantification by

Olympus Microsuite software. These measurements were then averaged for each heart, and

the results were expressed in square microns (µm) ± standard deviation (SD).

Table 5. Antibodies used in Western blotting experiments.

Antibody	Vendor	Cat. No.
4EBP1	Cell Signalling	9452
phospho-4EBP1 (Thr37/46)	Cell Signalling	2855
Akt 1/2	Santa Cruz	sc-1619
phospho-Akt (Ser473)	Cell Signalling	9271
ATG5	Cell Signalling	2630
Atrogin-1/MAFbx	ECM Biosciences	AP2040
beclin-1	Cell Signalling	3738
FoxO3a	Cell Signalling	9467
phospho-FoxO3a (Ser253)	Cell Signalling	9466
GAPDH	Fitzgerald	10R-G109a
GSK-3β	Cell Signalling	9315
phospho-GSK-3β (Ser9)	Cell Signalling	9323
mTOR	Cell Signalling	2972
phospho-mTOR (Ser2448)	Cell Signalling	2971
MuRF1	Abcam	ab77577
p70S6K	Cell Signalling	9202
phospho-p70S6K (Thr389)	Cell Signalling	9206

Chapter 5: RESULTS

5.1. Model of Left Ventricular Hypertrophy.

All animals completed the study except for one rat from the 14-day group that died at day 12 post-surgery.

5.1.1. Hemodynamic Screening by Doppler. Animals underwent hemodynamic evaluation by Doppler, prior to sacrifice (at 7 and 14 days post-banding or sham-operation), to screen for successful banding at the ascending aorta. Because sham pressure measurements served as parallel controls, we did not deem it necessary to perform any baseline studies.

The peak jet velocity, measured across the stenosis at the aortic arch, was greatly increased in rats whose ascending aorta was banded (RAAB). **Figure 8A** depicts representative images of the normal aspect of the aortic jet flow in a sham-operated and a RAAB at 14 days post surgery. At 7 days post-surgery, RAAB displayed an almost three-fold increase in the peak jet velocity measured across the stenosis at the aortic arch, compared to controls (2.88±0.52m/s vs. 1.01±0.06m/s, $p<0.01$; **Figure 8B**). At 14 days post-surgery, the RAAB displayed a greater than four-fold increase in the peak jet velocity across the stenosis at the aortic arch, compared to controls (4.24±0.34m/s vs. 1.09±0.12m/s, $p<0.01$, **Figure 8B**). Estimate of the pressure gradient (ΔP) across the stenosis by use of the simplified Bernoulli's equation yield an average increase of 34.2±11.9 and 72.5±11.1 mmHg for the 7-day and 14-day banded groups, respectively.

The peak velocity flow of both the right and left carotid arteries was expected to be lower in the banded animals, compared to controls, given the proximal placement of the band and was thus performed as routine. However, by 14 days post-banding, the RAAB displayed a consistent pattern of blunting of the peak flow of the right carotid artery combined with a sharp increase in the peak of the left carotid artery (**Figure 9A**). This
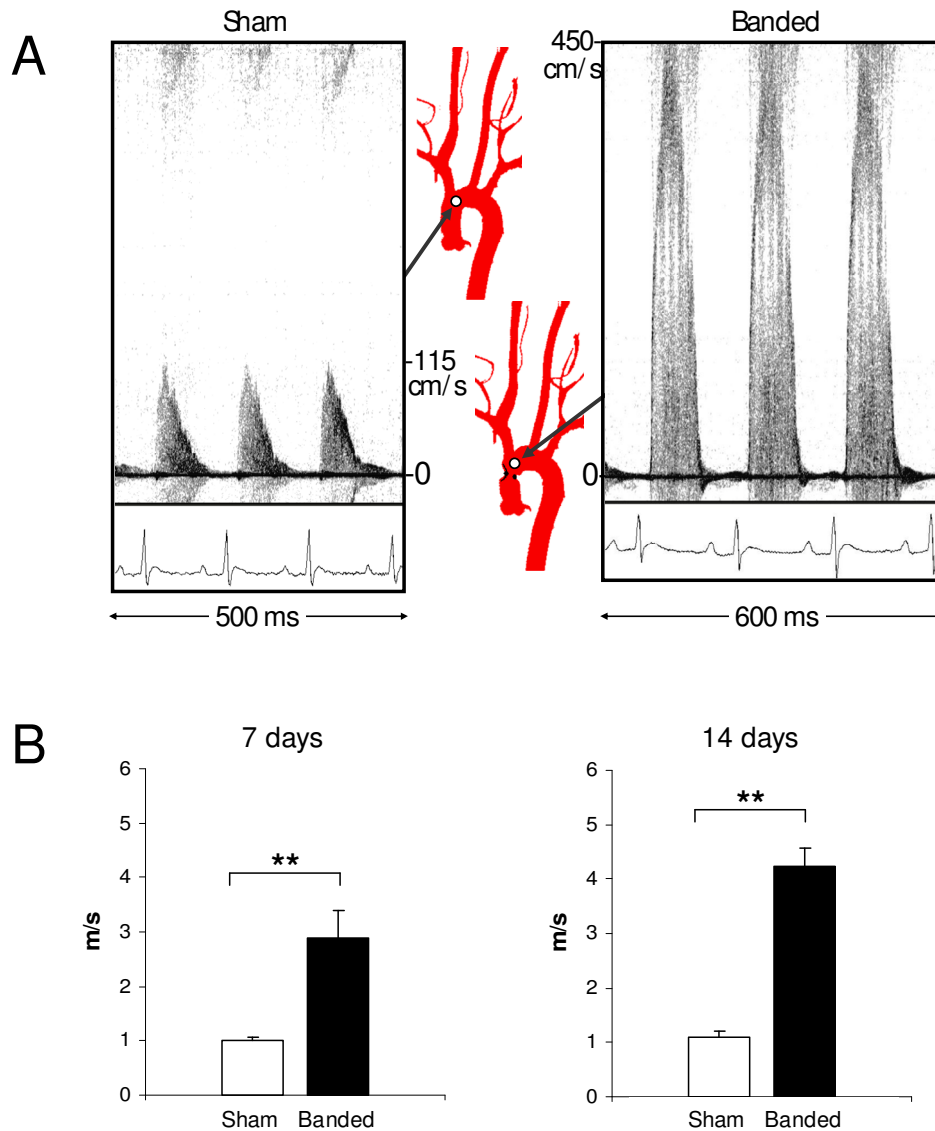
Figure 8. Doppler measurement of the peak stenotic jet velocity flow across the transverse portion of the aortic arch. **(A)** Representative images of the normal aspect of the aortic jet flow in a sham-operated rat (*left*) and a RAABs (*right*) at 14 days post surgery. **(B)** A three- and four-fold increase was observed across the stenosis in RAABs (n=8), compared to controls (n=5), at 7 and 14 days post-surgery, respectively. **p<0.01.
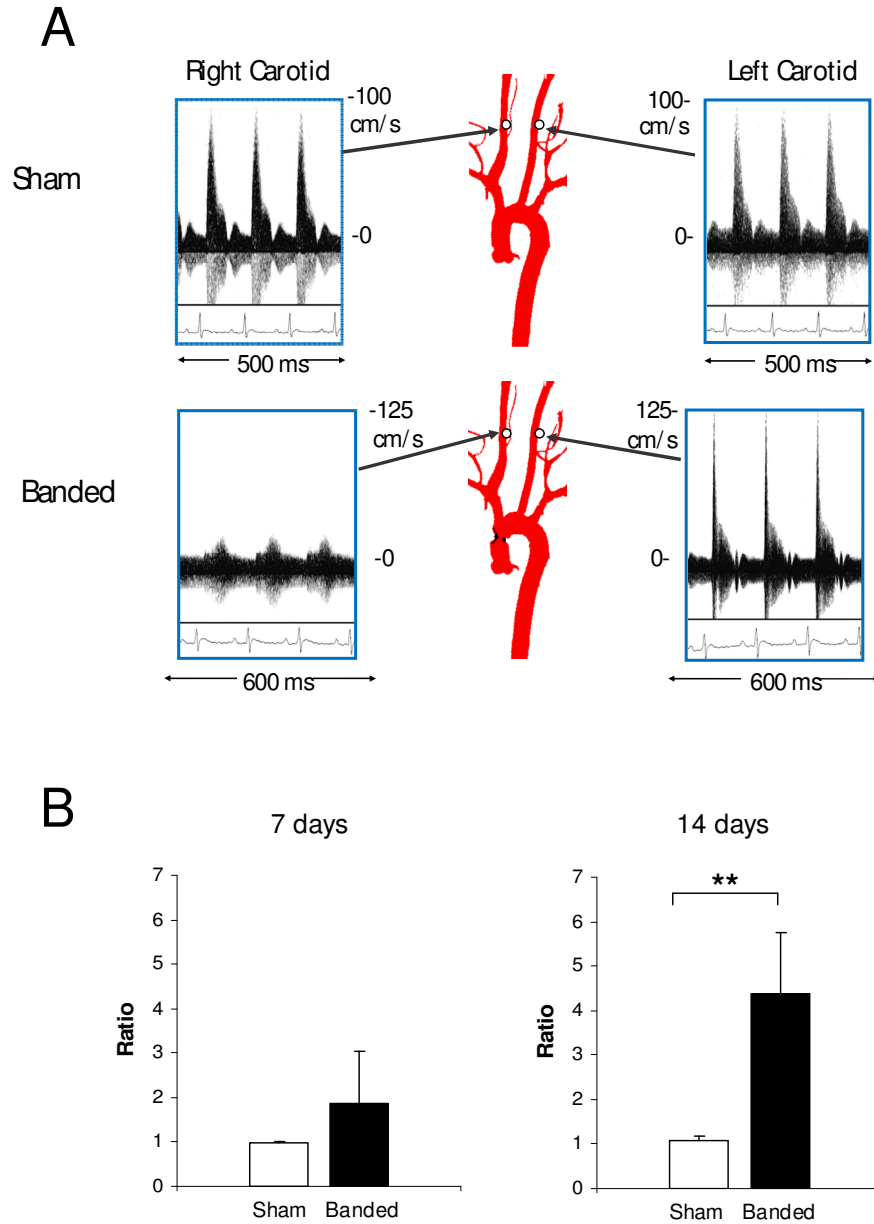
Figure 9. Doppler measurement of carotid flow. **(A)** Representative images of the normal aspect of the carotid peaks in a sham-operated rat (*top*) and the distinct pattern observed in banded rats (*bottom*) at 14 days post surgery. **(B)** Left/right carotid peak velocity ratios in RAABs (n=8), compared to controls (n=5), at 7 and 14 days post-surgery. **p<0.01.

resulted in a statistically significant increase in the left/right carotid velocity ratio between banded and sham-operated animals (4.4±1.36 vs. 1.08±0.11, p<0.01; **Figure 9B**). Carotid artery measurements at 7 days displayed considerable variability and comparison of the left/right carotid velocity ratio between RAAB and sham-operated rats did not reach statistical significance (1.88±1.17 vs. 0.97±0.04, p=NS; **Figure 9B**). These results indicate a successful and significant induction of aortic constriction at both time points.

5.1.2 Morphometric Assessment. I wanted to know whether increased left ventricular pressure also induced left ventricular hypertrophy in my model. Morphometric analyses were performed with respect to heart weight (HW)-to-body weight (BW) ratios, gross anatomy and histology (**Table 6**).

Table 6. Summary of morphometric assessments.

	7 days		14 days	
	Sham	Banded	Sham	Banded
HW/BW Ratio	✔	✔	✔	✔
Gross Anatomy	(✔)	(✔)	(✔)	(✔)
Histology	✔	✔	✔	✔

✔   Quantitative measurements
(✔) Representative images

After sacrifice at the respective time points of 7 and 14 days post-ascending aortic banding or sham-operation, hearts were excised and weighed. Heart weight to body weight (HW/BW) ratios were calculated to estimate the degree of cardiac hypertrophy. At 7

days post-banding, 3 of 8 animals showed less than a 10% increase in HW/BW ratio compared to controls and were, therefore, not included in the study.

At 7 days post-banding, the 5 hypertrophied hearts showed significant increase in their HW/BW ratio compared to controls ($4.28 \pm 0.54 \times 10^{-3}$ vs. $3.34 \pm 0.31 \times 10^{-3}$, $p<0.05$; **Figure 10A**). This increase was maintained and surpassed in the 14-day group, compared to controls ($4.68 \pm 0.47 \times 10^{-3}$ vs. $3.46 \pm 0.15 \times 10^{-3}$, $p<0.01$; **Figure 10B**). The average percent hypertrophy at 7 and 14 days post-banding was 29.4% and 35.1%, respectively (**Figure 10C**). Thus, at both time points, I was able to document an increase in left ventricular mass.

Two of the hearts in the 7-day group, and approximately one third of the hearts in the 14-day group showed gross changes in the normal anatomy, such as dilatation and enlargement of the left atrium (**Figure 11**). This observation was made by visual inspection only (no measurements were made) during the course of harvesting and freeze-clamping the hearts for further work-up (RNA and protein extraction).

5.1.3. Histology. With the documented increase in LV mass, I now wanted to find out whether the increase in LV mass was due to an increase in cell size (hypertrophy). From the subset of animals designated for histological evaluation, one rat from the 14-day group died 2 days before sacrifice.

Upon cross section of the heart perpendicular to its longitudinal axis, hearts from RAABs showed signs of concentric hypertrophic remodeling (**Figure 12**). In addition, the same hearts at both 7 and 14 days post-surgery also showed a marked increase in myocyte size compared to controls, as demonstrated by measurement of their cross-sectional area ($483 \pm 147 \mu m^2$ and $479 \pm 85 \mu m^2$ vs. $240 \pm 64 \mu m^2$, $p<0.01$, **Figure 13**). Hearts from RAABs

A

	7 days	
	Sham	**Banded**
BW (g)	259 ± 12	234 ± 11
HW (mg)	866 ± 107	1000 ± 130
HW/BW (x1000)	3.34 ± 0.31	4.28 ± 0.54

B

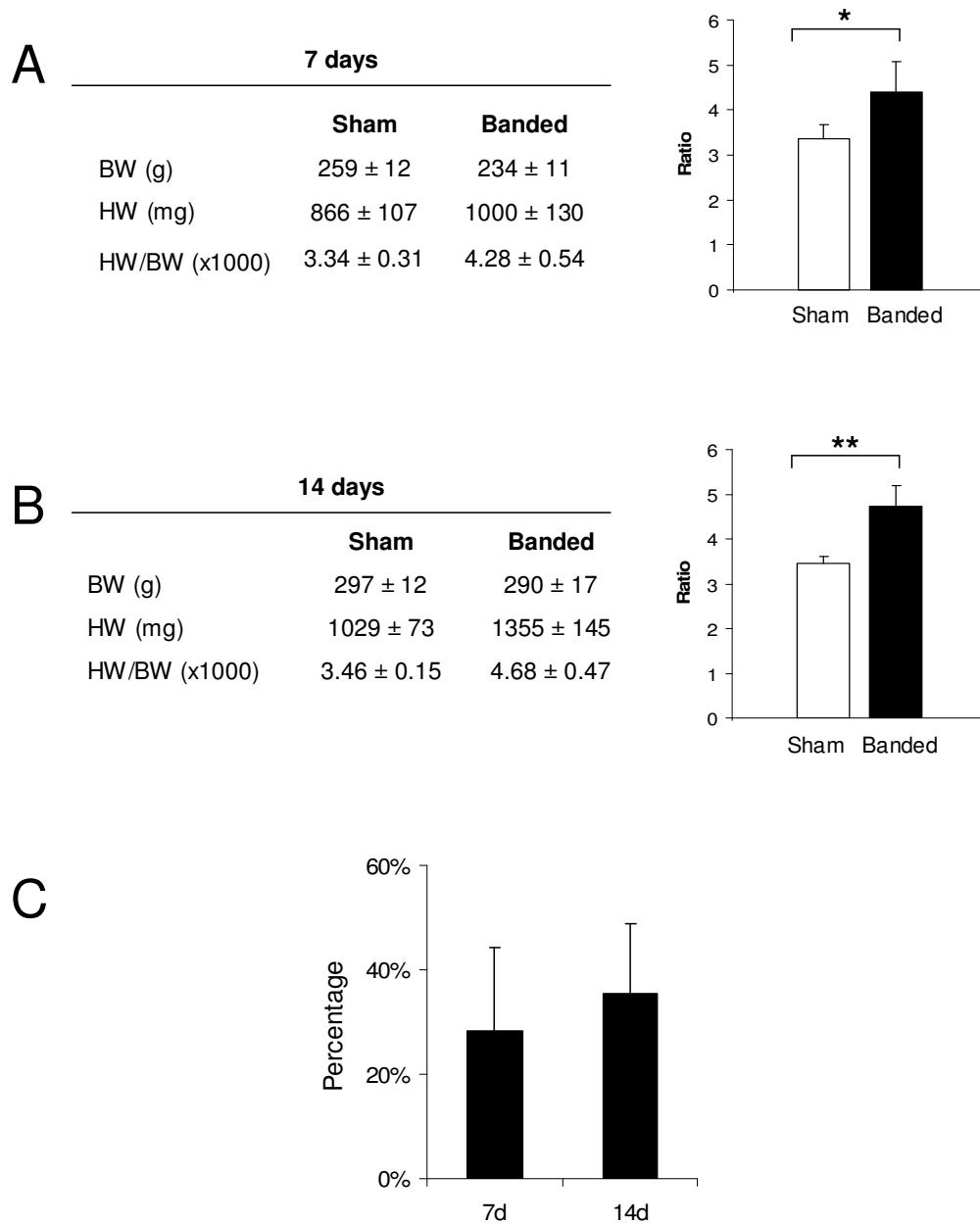|	**14 days**	
	Sham	**Banded**
BW (g)	297 ± 12	290 ± 17
HW (mg)	1029 ± 73	1355 ± 145
HW/BW (x1000)	3.46 ± 0.15	4.68 ± 0.47

C

Figure 10. Morphometric measurements. HW/BW ratios in RAAB (n=8) compared to controls (n=5), at **(A)** 7 and **(B)** 14 days post-surgery. **(C)** Percent hypertrophy at 7 and 14 days post-banding. BW = body weight, HW = heart weight, *p<0.05, **p<0.01.
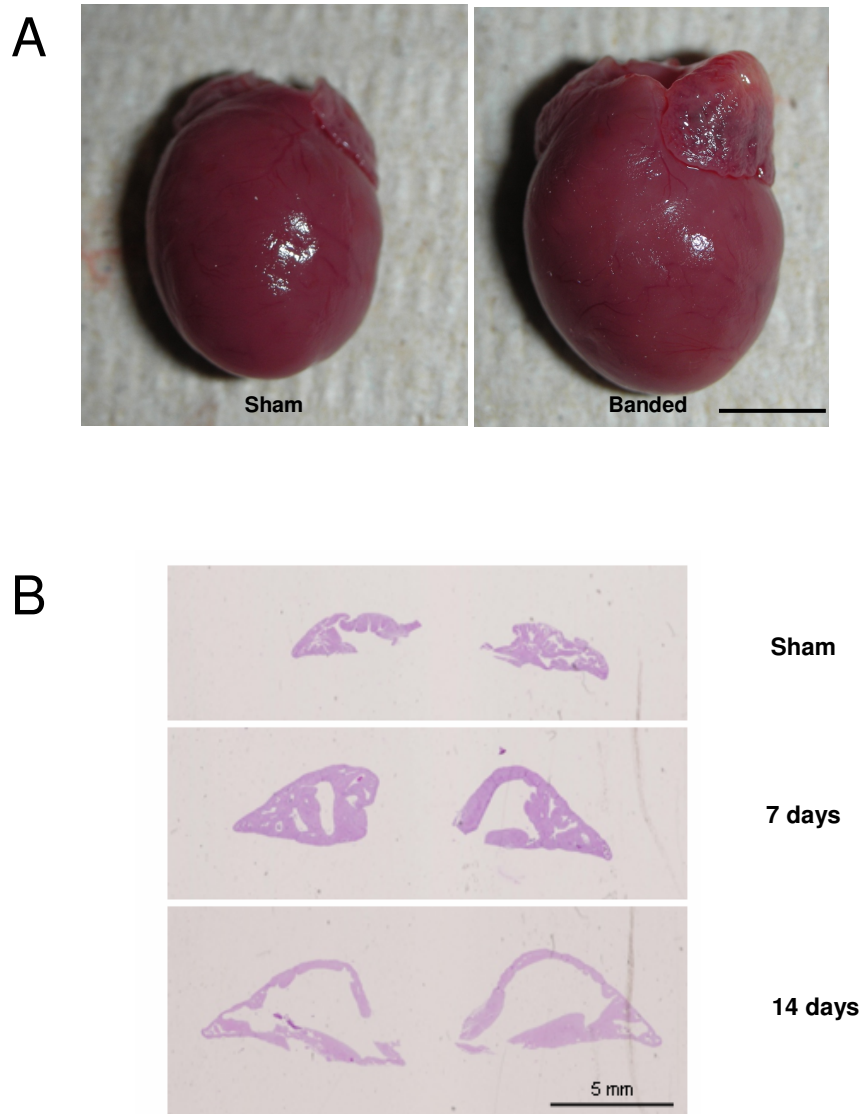
Figure 11. Gross changes in the hearts of RAAB. **(A)** Image of a rat heart at 14 days post-banding displaying marked hypertrophy, compared to control, and showing enlargement and dilation of the left atrium. **(B)** Histologic sections displaying the outline of normal (*top*) right atrium compared to the left atrium of a 7- (*middle*) and 14-day (*bottom*) post-banded rat. H&E stain. Bar = 5 mm.
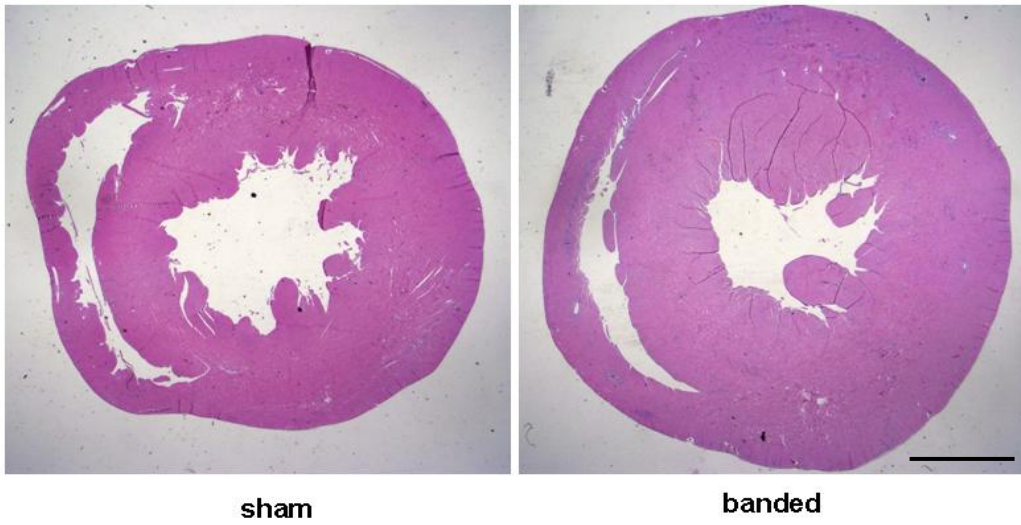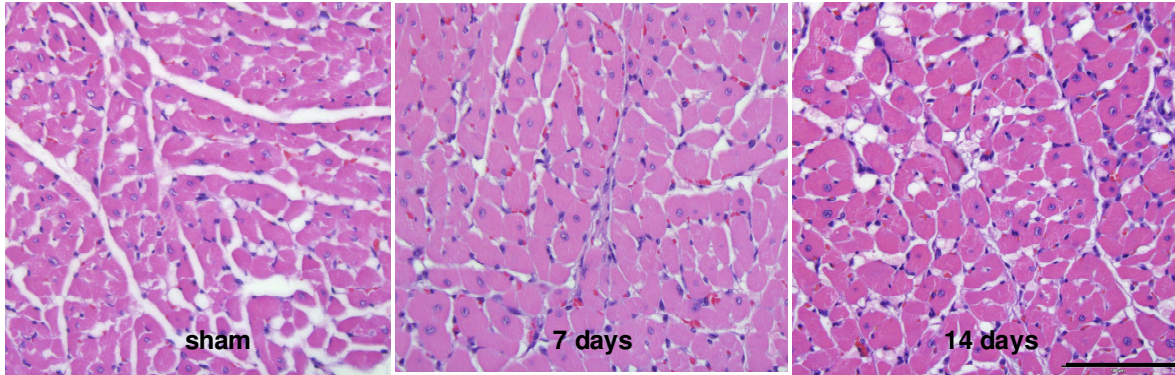
Figure 12. Histology. Cross-section of a heart from a sham-operated rat and a RAAB (7 days). Bar = 2mm.

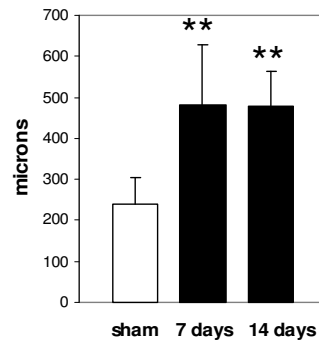**Figure 13.** Histology: myocyte size. **(A)** H&E image from a sham-operated, 7-day and 14-day RAAB displaying increase myocyte size in the banded rat heart. Bar = 100μm. **(B)** Quantification of myocyte cross-sectional area, **p<0.01.
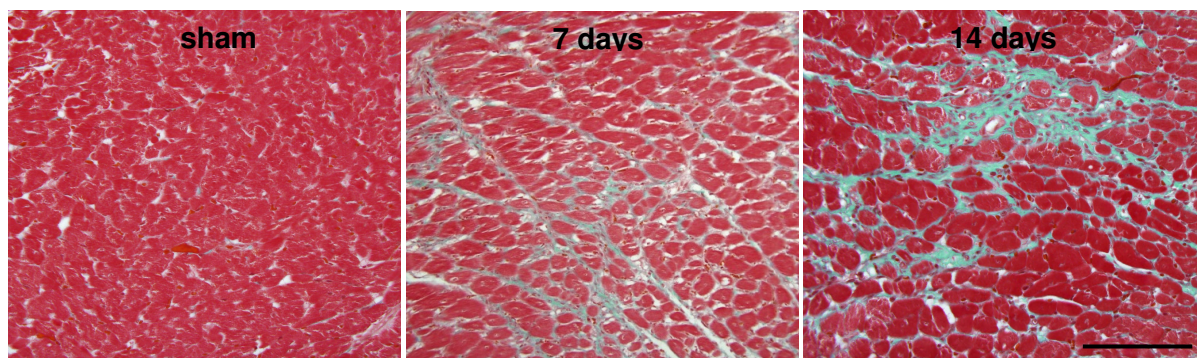
Figure 14. Histology: fibrosis. Trichrome stain showing increased collagen deposition in the heart of a 7 and 14-day RAAB compared to a sham-operated one. Bar = 100µm.

also displayed an increase in fibrosis, which was mostly interstitial, at both time points (**Figure 14**).

5.1.4 Transcript Analyses: Selected Markers of the Fetal Gene Program. A hallmark of cardiac remodeling is the return to the fetal gene program (Depre and others 1998; Rajabi and others 2007; Taegtmeyer and others 2010). To further characterize and confirm achievement of a successful model of left ventricular pressure overload, we assessed level of key transcripts known to shift in the stressed heart.

We first assayed for atrial natriuretic factor (ANF) because it is a marker of cardiac remodeling and heart failure. ANF levels were considerably increased in banded hearts compared to controls, at both 7 days (2.4 ± 0.99 x10^6 vs. 0.29 ± 0.04 x10^6 copies/total RNA, $p<0.05$) and 14 days post-banding (3.8 ± 0.46 x10^6 vs. 0.29 ± 0.04 x10^6 copies/total RNA, $p<0.01$).

We next assayed for markers of isoform switches, also well described in cardiac remodeling (Depre and others 1998). An expected switch is the myosin heavy chain isoforms, characteristic of a return to the fetal gene program, was also observed in banded hearts compared to controls. MHC-α was significantly downregulated in banded hearts compared to controls at both 7 days (2.44 ± 0.38 x10^8 vs. 4.6 ± 0.33x10^8 copies/total RNA, $p<0.01$) and 14 days post-surgery (1.43 ± 0.19 x10^8 vs. 3.0 ± 0.49x10^8 copies/total RNA, $p<0.01$). Reversely, MHC-β was significantly upregulated in banded hearts compared to controls at both 7 days (3.47 ± 1.16 x10^5 vs. 1.25 ± 0.23x10^5 copies/total RNA, $p=0.05$) and 14 days post-surgery (7.42 ± 0.19 x10^5 vs. 1.07 ± 0.21x10^5 copies/total RNA, $p<0.01$). **Figure 15** displays the results in graphic form.
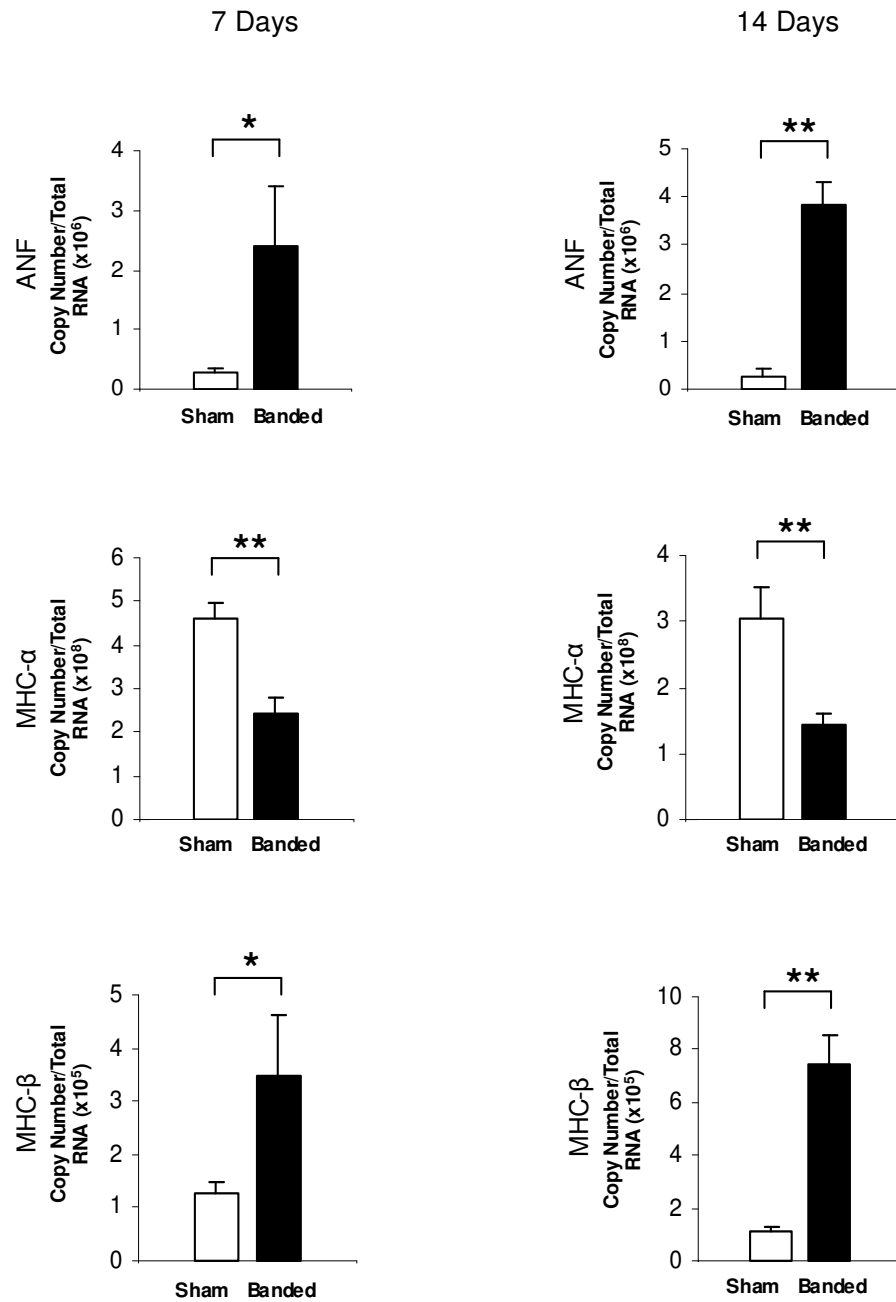
Figure 15. qRT-PCR results: The fetal gene program is activated during pressure overload. At both time points, 7 days *(graphs on left)* and 14 days *(graphs on right)* ANF is markedly elevated and there is a classic isoforms switch of the MHCs α nd β. Results are shown as mean±SE. Banded (n=5 and n=8 at 7 and 14 days post-surgery, respectively); sham (n=5), *p<0.05, **p<0.01.

5.2 Focused Analysis of the UPS

5.2.1 20S Proteasome Activity Assay. We also wanted to know whether proteasome activity

had changed following hemodynamic pressure overload in the left ventricle at either time

points. The 20S proteasome activity assay (previously described above under Methods, page

23) showed no difference between the left ventricular tissue lysates from RAABs compared

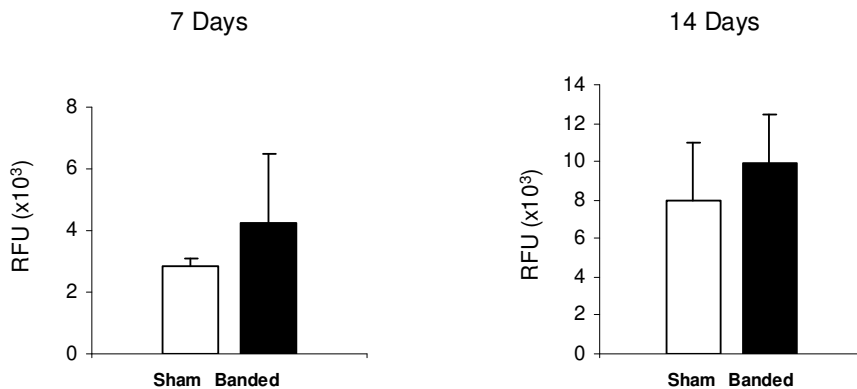to shams, at either 7 or 14 days post-banding (**Figure 16**).

Figure 16. Results from the 20S proteasome activity assay. Samples were run in duplicates. Fluorescence units were normalized to protein concentration. RFU = relative fluorescence units.

5.2.2. Transcript analysis: MAFbx, MuRF1 and PSMB4. Transcript analysis of the E3

liagses, MAFbx and MuRF1, showed that MAFbx was significantly decreased in RAAB

hearts at 7 days post-surgery compared to controls ($6.12\pm0.33\text{x}10^5$ vs. $7.43\pm0.34\text{x}10^5$

copies/total RNA, p<0.05). However, this downregulation was not maintained in the 14-day

banded hearts ($1.56\pm0.08\text{x}10^5$ vs. $1.71\pm0.1\text{x}10^5$ copies/total RNA, p=NS). On the other

hand, the E3 ligase MuRF1 did not display any significant difference between the banded

and sham-operated hearts at either 7 days ($4.92\pm0.29\text{x}10^4$ vs. 4.35 ± 0.21 $\text{x}10^4$ copies/total

RNA, p=NS) or 14 days post-surgery ($2.46\pm0.16\text{x}10^4$ vs. $2.71\pm0.16\text{x}10^4$ copies/total RNA,

p=NS), compared to controls (**Figure17**).

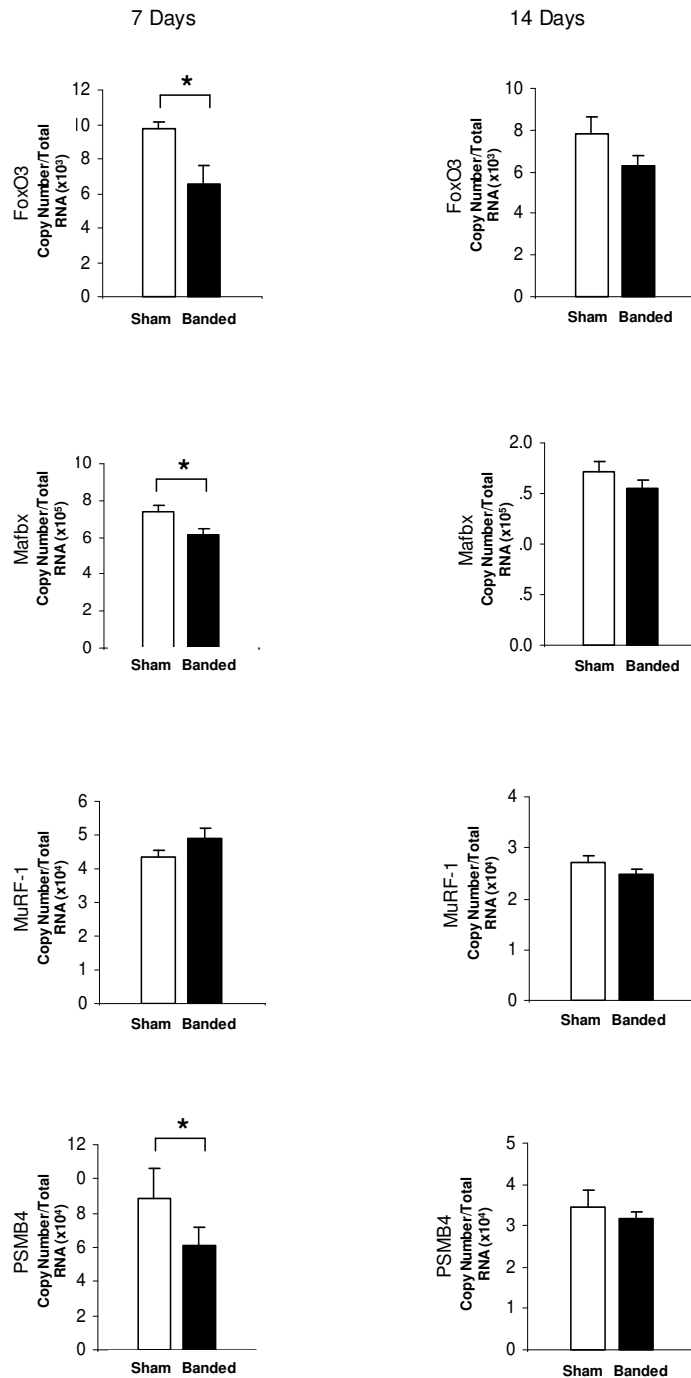**Figure 17.** UPS and FoxO3a transcript levels are decreased by the first week of pressure overload-induced hypertrophy. FoxO3a and all of the UPS components analyzed, except MuRF1, appear decreased after 7 days of ascending aortic banding. This effect is no longer observed after 14 days. Results are shown as mean±SE. Banded (n=5 and n=8 at 7 and 14 days post-surgery, respectively); sham (n=5), *p<0.05, **p<0.01.

The marker for one of the catalytic subunits of the proteasome, PSMB4, also appeared significantly decreased in banded hearts at 7 days post-surgery compared to controls ($6.1\pm0.85\times10^4$ vs. $8.84\pm0.61\times10^4$ copies/total RNA, p<0.05). However, as in the case of MAFbx, this downregulation was not maintained in the 14-day banded hearts ($3.15\pm0.19\times10^4$ vs. $3.45\pm0.43\times10^4$ copies/total RNA, p=NS). **Figure 17**.

5.2.3. Protein Expression: MAFbx/Atrogin-1, MuRF1.

In order to confirm changes in transcript levels, we also performed protein analysis by Western blot. MAFbx did not show significant changes compared to controls at either 7 days (0.72 ± 0.13 vs. 0.7 ± 0.1 arbitrary units, p=NS) or 14 days after banding (0.45 ± 0.29 vs. 0.52 ± 0.14 arbitrary units, p=NS). As in the case of MAFbx, MuRF1 also displayed non-significant protein expression after densitometric analysis after for both 7 days (0.53 ± 0.03 vs. 0.51 ± 0.11 arbitrary units, p=NS) and 14 days after banding (0.29 ± 0.08 vs. 0.33 ± 0.05 arbitrary units, p,0.05) compared to controls. **Figures 18, 19**.

5.3 Regulation of the UPS

5.3.1 FoxO3a. The transcription factor FoxO3a was noticeably downregulated in banded hearts at 7 days post-surgery compared to controls ($6.54\pm1.11\times10^3$ vs. $9.75\pm0.4\times10^3$ copies/total RNA, p<0.05). This downregulation remained only as a trend in banded hearts by 14 days post-surgery, compared to controls ($6.3\pm0.52\times10^3$ vs. $7.79\pm0.83\times10^3$ copies/total RNA, p=0.07).

FoxO3a showed no significant changes in phosphorylation at 7 days post banding (1.07 ± 0.37 vs. 0.83 ± 0.69 arbitrary units, p=NS), and a significant decrease at 14 days after banding (1.12 ± 0.2 vs. 0.62 ± 0.48 arbitrary units, p=0.05). (**Figures 17** and **20**).

5.3.2 *The Akt/mTOR pathway.* In addition, we performed Western blots of relevant components of this pathway of protein synthesis.

p-Akt (Ser473) was significantly increased after 7 days of banding, compared to controls ($1.01.63\pm0.03$ vs. 0.62 ± 0.17 arbitrary units, $p<0.05$), and significantly decreased at 14 days after banding (0.46 ± 0.11 vs. 0.95 ± 0.12 arbitrary units, $p<0.05$). Western blot analysis was also performed on other downstream members of this pathway, such as p-mTOR (Ser2481), p-4EBP1 (Thr37-46), p-p70S6K (Thr389) and p-GSK-3β (Ser9). These markers all showed a modest trend towards elevation at 7 days post banding and normalization by 14 days post-banding, but statistical significance was not reached (data not shown).

5.4 Autophagy

Beclin-1 was non-significant after 7 days of banding, compared to controls (1.06 ± 0.49 vs. 1.28 ± 0.09 arbitrary units, $p=NS$), as well as at 14 days after banding (0.78 ± 0.26 vs. 0.63 ± 0.22 arbitrary units, $p=NS$). ATG5 was non-significant after 7 days of banding, compared to controls (0.88 ± 0.43 vs. 0.89 ± 0.21 arbitrary units, $p=NS$), as well as at 14 days after banding (1.08 ± 0.54 vs. 1.29 ± 0.11 arbitrary units, $p=NS$). **Figure 22**.
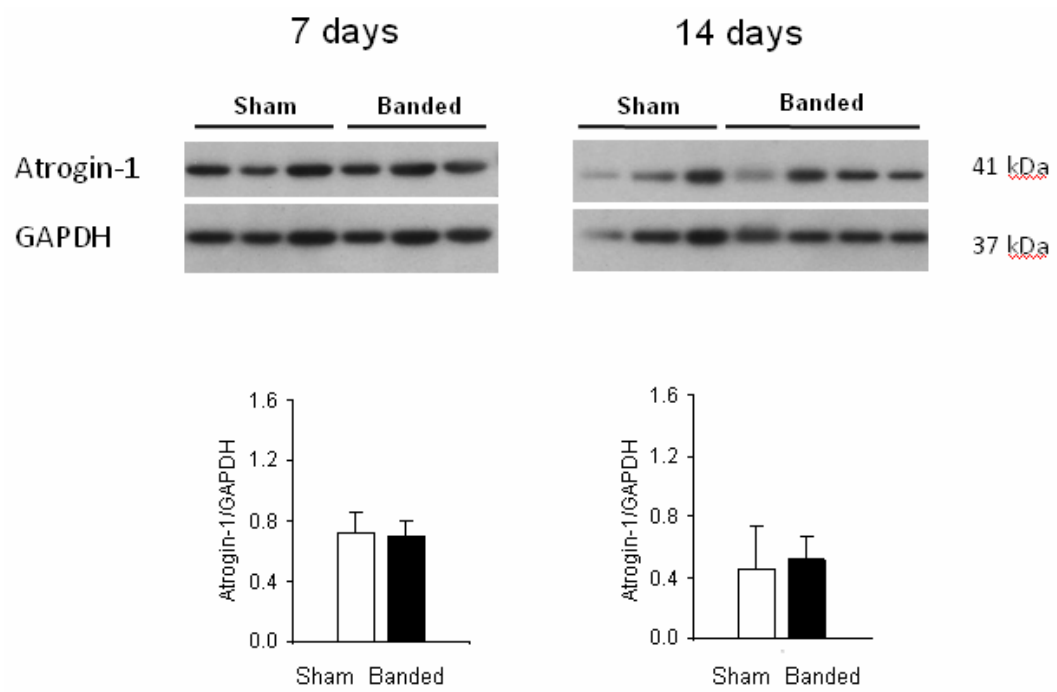
Figure 18. Atrogin-1 protein expression at 7 and 14 days post banding. No significant difference was noted at either time point compared to controls.
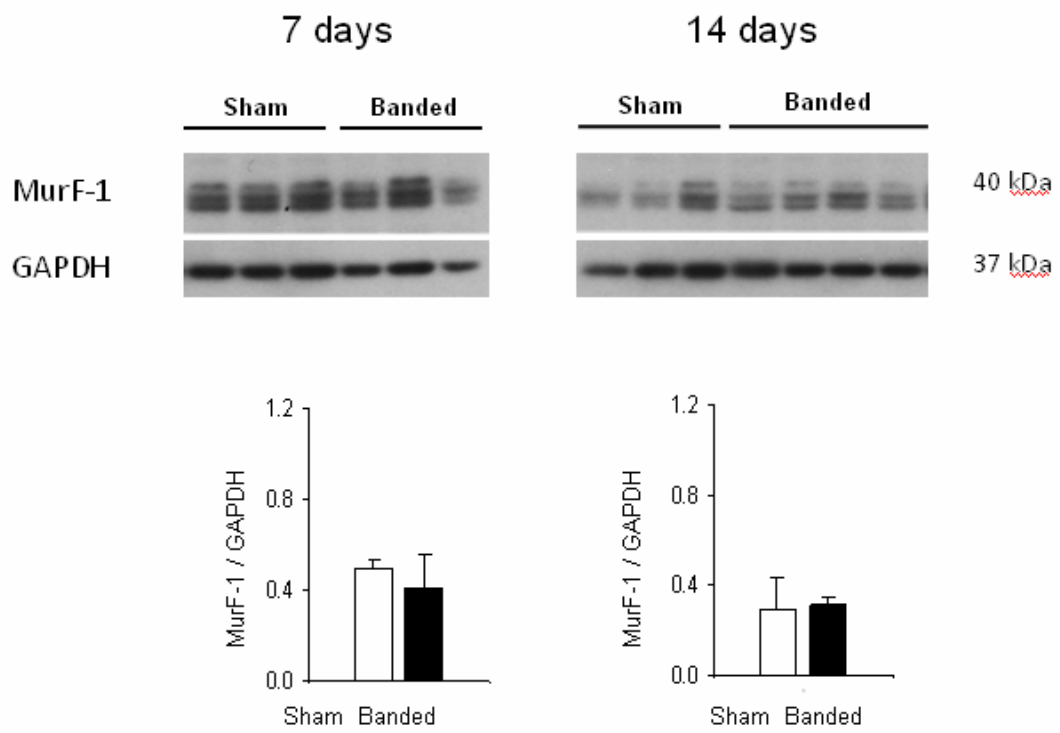
Figure 19. MuRF-1 protein expression at 7days and 14 days post banding. No significant difference was noted at either time point compared to controls.
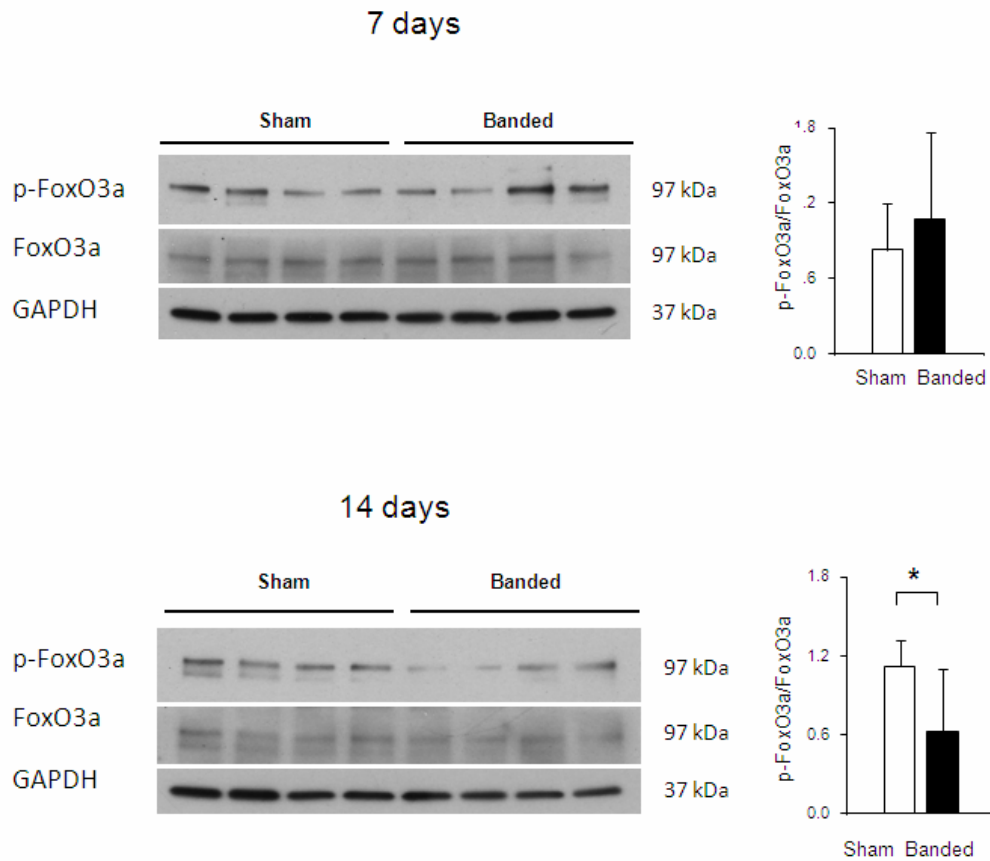
Figure 20. FoxO3a protein expression at 7 and 14days post banding. FoxO3a showed no significant changes in phosphorylation at 7 days post banding (1.07±0.37 vs. 0.83±0.69 arbitrary units, p=NS), and a marginally significant decrease at 14 days after banding (1.12±0.2 vs. 0.62±0.48 arbitrary units, *p=0.05).
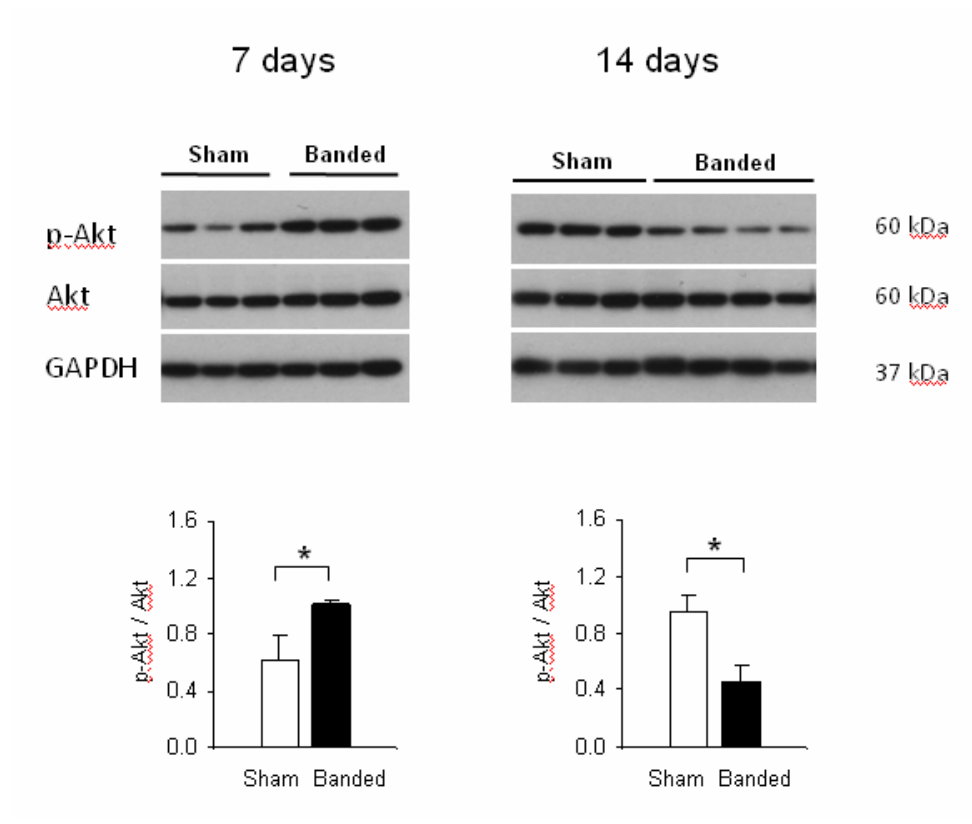
Figure 21. Akt protein expression at 7 and 14 days post banding. p-Akt (Ser473) was significantly increased at after 7 days of banding, compared to controls (1.01.63±0.03 vs. 0.62±0.17 arbitrary units), and significantly decreased at 14 days after banding (0.46±0.11 vs. 0.95±0.12 arbitrary units), *p<0.05.
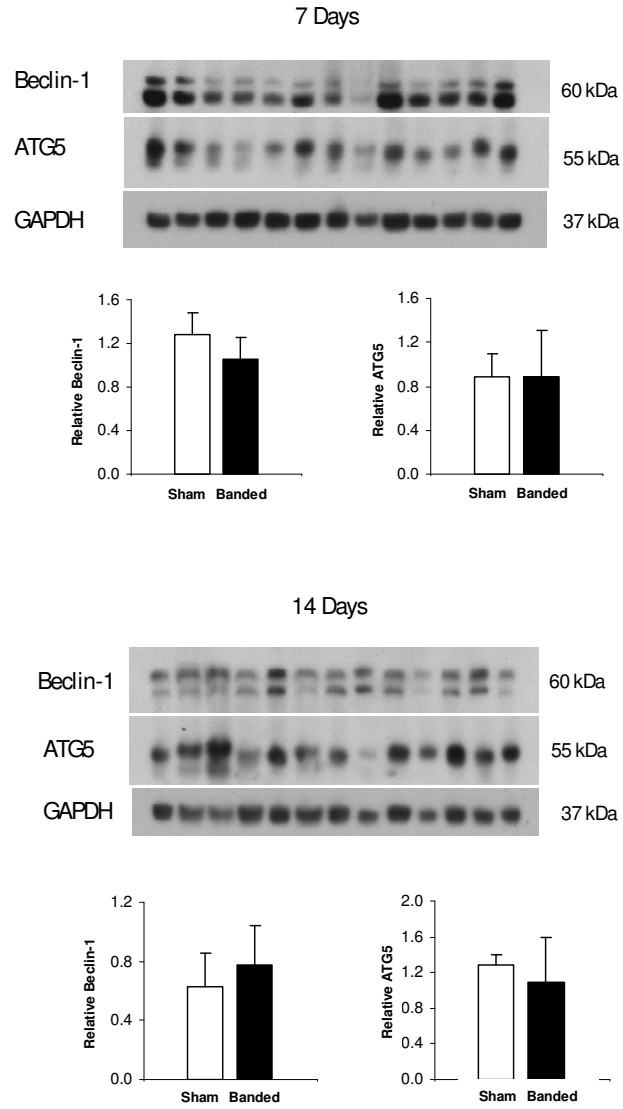
Figure 22. Autophagy protein expression at 7 and 14 days post-banding shows no difference between banded and controls. Results are shown as mean±SD. Banded (n=5 and n=8 at 7 and 14 days post-surgery, respectively), sham (n=5), *p<0.05, §p=0.05.

Table 7. Summary of results.

	7 days		14 days	
	mRNA	*Protein*	*mRNA*	*Protein*
Fetal Gene Program				
ANF	↑		↑↑	
MHC-α	↓		↓	
MHC-β	↑		↑↑	
Akt		↑		↓
UPS				
FoxO3a	↓	ns	ns	↑
MAFbx	↓	ns	ns	ns
MuRF-1	ns	ns	ns	ns
PSMB4	↓		ns	
Proteasome Activity Assay		ns		ns
Autophagy				
beclin-1		ns		ns
ATG5		ns		ns

Chapter 6: DISCUSSION

In the preceding chapters I laid out the rationale and background for my hypothesis, described experimental approach and methods and reported results. The main findings from this study are summarized in **Table 7** on page 56. Banded rats showed a four-fold increase in peak stenotic jet velocities. Histomorphometric analysis revealed a significant increase of myocyte size as well as of fibrosis in the banded animals. Transcript analysis showed that banded animals had reverted to the fetal gene program. Transcript analysis revealed decreases in transcript levels of several candidate UPS genes in the hypertrophied hearts at 7 days post-banding but not at 14 days. However, protein expression analysis showed no difference at either time point compared to controls. I will now discuss the importance of my findings.

6.1 The UPS in the Hypertrophic Setting

Since its discovery in the late 1970s (Ciechanover and others 1980), the UPS has generated considerable interest as a main pathway of intracellular protein degradation and its role in health and disease (Ciechanover 2006). The discovery of muscle-specific E3 ligases (Bodine and others 2001; Gomes and others 2001), shared by both skeletal and cardiac muscle, was an important breakthrough specifically as it created interest regarding whether the UPS could play a role the in cardiovascular field as well. Within this context (see **Figure 4** in Chapter 3), given that the heart requires constant adaptation to environmental stressors in its environment, it was proposed that the UPS may play a role in the setting of cardiac remodeling underlying hypertrophy.

The results from my study that addressed the UPS show a biphasic pattern at 7 days and 14 days. In early hypertrophy (i.e. at 7 days post-banding), the transcript levels of E3 ligase MAfbx and the proteasome component PSMB4 appeared decreased compared to

sham-operated animals. At 14 days after banding, however, there was no difference in transcript levels (please see **Figures 4** and **5**, on pages 15 and 19, for the diagram of the UPS and proteasome). In contrast to Atrogin-1, MuRF-1 showed no changes at either time point. In addition, transcript levels of the transcription factor, FoxO3a, were decreased at 7 days post banding and showed a strong trend towards decreasing levels at 14 days post-banding. This means that mRNA levels change dramatically after aortic banding. It also means that a regulator of the UPS is dramatically downregulated as the heart hypertrophies.

To verify this observation, I also examined protein levels of the relevant UPS components by Western blot analysis. At the protein expression level, neither of the E3 ligases (Mafbx and MuRF-1) showed differences compared to sham-operated animals, nor did the proteasome activity assay (chymo-trypsin activity). The transcription factor FoxO3a showed only a trend towards increased phosphorylation (inactivation) at 7days post-aortic banding and marked decreased phosphorylation (activation) at 14 days. These findings in the UPS components were accompanied by an apparent increase in protein expression of several components of the Akt/mTOR signaling axis, indicators of increased protein synthesis and translation.

The disappearance of most of the significant 7-day findings by the 14-day time point, particularly at the transcript level, clearly indicates a shift towards a new steady state –and re-confirm the dynamic nature of the heart as it adapts to pressure overload. A possible explanation for these biphasic results may lie in the animal model of left ventricular hypertrophy (*discussed below*).

Regulation of the UPS in hypertrophy. The findings at the 7-day time point are consistent with the work of other researchers (Bodine and others 2001b; Kops and others 1999; Latres

and others 2005; Meier and others 1997; Skurk and others 2005). In an *in vitro* model of stretch-induced hypertrophy in cardiomyocytes, Skurk et al. showed that transduction with FoxO3a effectively activates atrophy-related genes, but treatment with constitutively active Akt suppressed this effect (Skurk and others 2005). The authors concluded that while FoxO3a can activate an "atrogene" transcriptional program in cardiomyocytes, this program is ultimately down-regulated by multiple physiologic and pathologic growth pathways. In another study, Stitt et al. showed that the IGF-1/PI3K/Akt pathway prevents the induction of the ubiquitin ligases MAFbx and MuRF1. The authors concluded that this occurs by Akt-mediated inhibition of the FoxO family. Both of these studies were performed in isolated cardiomyocytes. My results prove this now in an *in vivo* model.

Down-regulation of the atrogene program by growth signaling pathways has been observed in skeletal muscle as well (Bodine and others 2001b; Latres and others 2005). There is also cumulative documentation of the Akt inhibitory effect on the FoxO family (Kops and others 1999; Meier and others 1997). The presence of the non-phosphorylated transcription factor FoxO3a is required in the nucleus for the upregulation of the E3 ligases MAFbx and MuRF1. In the setting of an activated PI3K/Akt axis, PI3K phosphorylation of Akt causes it to translocate into the nucleus where it phosphorylates FoxO. Once in the nucleus, phosphorylation of FoxO by Akt causes its translocation into the cytoplasm where it can no longer exert its effect in the activation of MAFbx and MuRF1 (Brownawell and others 2001; Glass 2005; Ronnebaum and Patterson 2010).

We can thus conclude that MAFbx and MuRF1 may exert their effects, only in the degree to which they are released from the inhibitory hold of Akt. The hierarchal relationship between an activated PI3K/Akt growth pathway (as in the case of hypertrophy)

and the UPS is that in favor of PI3K/Akt dominance. This is illustrated by the diagram in **Figure 23**.

An additional, and very interesting, observation garnered from the results of my study is that MAFbx and MuRF1 could potentially be differentially regulated. At the transcript level, my data show that MAFbx follows its transcription factor FoxO3a closely. However, MuRF1 does not. The literature in this regard is still very scarce (Attaix and Baracos 2010) and holds the potential for new discoveries. In skeletal muscle, activation of the NF-κB pathway has been linked to exclusive transcriptional upregulation of MuRF1 while Mafbx/Atrogin-1 was not perturbed (Cai and others 2004; Hunter and Kandarian 2004). It was also shown that induction of proteasome expression could be diminished by inhibiting NF-κB activity (Wyke and others 2004). MAFbx/Atrogin-1 has been linked to the
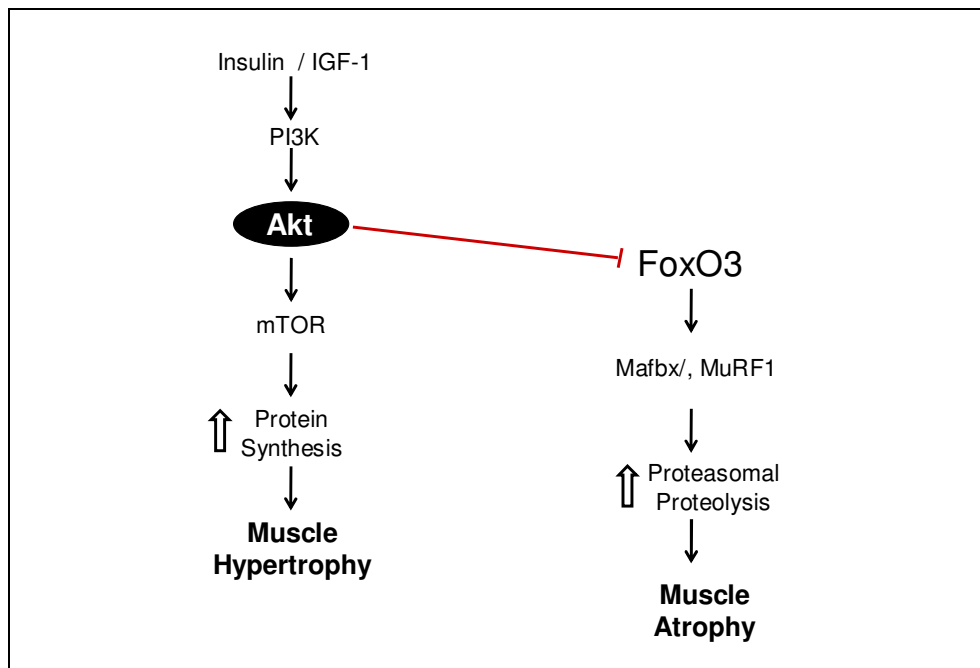

Figure 23. Regulation of muscle protein breakdown during hypertrophy and Atrophy. Adapted, with permission, from *Autophagy* (Zhao and others 2008).

TNFa pathway via activation of p38 (Li and others 2005). It remains to be seen if a similar regulation is relevant in the heart.

In conclusion, a successful model of left ventricular pressure overload was produced, at least for my first time point. However, based on the results from my experiments, the UPS does not appear to be a predominant figure in early hypertrophy due to inhibition by the PI3K/Akt/mTOR pathway.

Other pathway markers of intracellular protein degradation. In addition to examining the UPS as an indicator of protein degradation activity during hypertrophy, we also we also examined the protein expression of two key elements of the autophagy pathway, beclin-1 and ATG5 (**Figure 8** on page 25). This choice was due to a recent publication making a point of a link in the activation of the proteasome and autophagic pathway by FoxO3a (Zhao and others 2008). Our laboratory has also recently reported that markers of autophagy decrease in the failing heart with mechanical unloading [Kassiotis and others 2009]. In this study I have found no change in these markers. This most likely means that autophagy is not increased during early hypertrophy.

6.2 Model of LV hypertrophy vs. heart failure

As stated on numerous occasions throughout this dissertation, the heart is constantly adapting to its environment and various stimuli thanks to the dynamic nature of its constituents. This basic notion becomes very relevant in considering an animal model to stress the heart. While our main goal has been to produce a robust model of left ventricular pressure overload, there are considerations (or pitfalls) in regards to the shifting nature of this pathophysiological state: the transition from a compensated hypertrophy to heart failure.

Our model, at the transcript level, showed classic induction of the fetal gene program at both time points (please refer to Chapter 2 for more on the fetal gene program). This finding positively corroborates that our model is robust and that we successfully stressed the heart via pressure overload. Nonetheless, the LV hypertrophy -which resulted predominantly as concentric, as evidenced by morphologic assessment (**Figure 8**, page 37 of Results)- also appeared to develop extremely quickly. This abrupt and very intense induction of hypertrophy can be efficiently sustained by early functional compensation. However, it is a known outcome that maladaptive changes at the molecular, biochemical, and metabolic level will ultimately lead the heart muscle into failure (Grossman and others 1975; Meerson 1969).

It is difficult to assert that our model was in fact already progressing into failure in our current study and can appear purely speculative in lieu of having performed an echocardiographic assessment on the subject. Nonetheless, in a recent publication, Li et al. followed the transition of several survival signaling pathways in a mouse model of hypertrophy (transaortic constriction, TAC) as it progressed to heart failure (Li and others 2009). The authors found an increase in Akt and GSK-3β phosphorylation early in hypertrophy, followed by a decrease as the model progressed into failure. In addition, the histologic findings showed a pattern of interstitial myocardial fibrosis appear in the compensated hypertrophy, and later progress to replacement fibrosis as heart failure developed. These findings are similar to what we have observed at the 7 and 14 day time points, respectively.

In another recent study, Previlon et al. followed the sequential alterations on Akt and GSK-3β in a mouse model of aortic constriction (TAC) for 60 days (Previlon and others 2010). These authors also found an increase of Akt activity (phosphorylation) early in the

hypertrophic response, and the consequential GSK-3β inactivation (phosphorylation). These findings are also analogous to what we have observed at the protein expression level at the 7 and 14 days time points.

6.3 Concluding remarks

With the current interest in the UPS and its role in cardiovascular disease, numerous studies can be found in the literature, many of which appear to contradict the findings of this study (Depre and others 2006; Meiners and others 2008; Stansfield and others 2008). However, closer examination of this work reveals that these studies are either performed *in vitro*, in models of heart failure *in vivo*, or have utilized proteasome inhibition. Our study is unique in that it focuses exclusively on early hypertrophy.

The relevance of UPS and its profound implication in numerous human pathophysiological states in currently widely accepted. The results of our study indicate that the UPS is dynamically regulated at the transcriptional level. This is evidenced by a biphasic display of mRNA levels in a hypertrophic setting, with early downregulation, followed by normalization. This dynamic response observed appears to be at least partially mediated by the pro-hypertrophic and growth pathway, the Akt/mTOR axis. In addition, the transcriptional shifts observed in mRNA levels did not, however, translate to the protein expression level. This discrepancy suggests the existence of a post-transcriptional regulation as well, the exact mechanism of which remains to be elucidated.

I consider that my study contributes to the current knowledge in the field by bringing forth: a) a temporal sequence of the UPS markers in the initiation and stabilization of hypertrophy, and b) the dynamic and hierarchal relationship between pro-hypertrophic and growth pathways.

References

Arcos JC, Sohal RS, Sun SC, Argus MF, Burch GE. 1968. Changes in ultrastructure and respiratory control in mitochondria of rat heart hypertrophied by exercise. Exp Mol Pathol 8(1):49-65.

Attaix D, Baracos VE. 2010. MAFbx/Atrogin-1 expression is a poor index of muscle proteolysis. Curr Opin Clin Nutr Metab Care 13(3):223-4.

Bodine SC, Latres E, Baumhueter S, Lai VK, Nunez L, Clarke BA, Poueymirou WT, Panaro FJ, Na E, Dharmarajan K and others. 2001a. Identification of ubiquitin ligases required for skeletal muscle atrophy. Science 294(5547):1704-8.

Bodine SC, Stitt TN, Gonzalez M, Kline WO, Stover GL, Bauerlein R, Zlotchenko E, Scrimgeour A, Lawrence JC, Glass DJ and others. 2001b. Akt/mTOR pathway is a crucial regulator of skeletal muscle hypertrophy and can prevent muscle atrophy in vivo. Nat Cell Biol 3(11):1014-9.

Brown L, Sernia C, Newling R, Fletcher P. 1992. Cardiac responses after norepinephrine-induced ventricular hypertrophy in rats. J Cardiovasc Pharmacol 20(2):316-23.

Brownawell AM, Kops GJ, Macara IG, Burgering BM. 2001. Inhibition of nuclear import by protein kinase B (Akt) regulates the subcellular distribution and activity of the forkhead transcription factor AFX. Mol Cell Biol 21(10):3534-46.

Buttrick PM, Scheuer J. 1987. Physiologic, biochemical, and coronary adaptation to exercise conditioning. Cardiol Clin 5(2):259-70.

Cai D, Frantz JD, Tawa NE, Jr., Melendez PA, Oh BC, Lidov HG, Hasselgren PO, Frontera WR, Lee J, Glass DJ and others. 2004. IKKbeta/NF-kappaB activation causes severe muscle wasting in mice. Cell 119(2):285-98.

Cao DJ, Gillette TG, Hill JA. 2009. Cardiomyocyte autophagy: remodeling, repairing, and reconstructing the heart. Curr Hypertens Rep 11(6):406-11.

Chomczynski P, Sacchi N. 2006. The single-step method of RNA isolation by acid guanidinium thiocyanate-phenol-chloroform extraction: twenty-something years on. Nat Protoc 1(2):581-5.

Ciechanover A. 2006. Intracellular protein degradation: from a vague idea thru the lysosome and the ubiquitin-proteasome system and onto human diseases and drug targeting. Exp Biol Med (Maywood) 231(7):1197-211.

Ciechanover A, Elias S, Heller H, Ferber S, Hershko A. 1980. Characterization of the heat-stable polypeptide of the ATP-dependent proteolytic system from reticulocytes. J Biol Chem 255(16):7525-8.

Dahl LK, Knudsen KD, Ohanian EV, Muirhead M, Tuthill R. 1975. Role of the gonads in hypertension-prone rats. J Exp Med 142(3):748-59.

De Duve C, Gianetto R, Appelmans F, Wattiaux R. 1953. Enzymic content of the mitochondria fraction. Nature 172(4390):1143-4.

Dean RT, Barrett AJ. 1976. Lysosomes. Essays Biochem 12:1-40.

Depre C, Shipley GL, Chen W, Han Q, Doenst T, Moore ML, Stepkowski S, Davies PJ, Taegtmeyer H. 1998. Unloaded heart in vivo replicates fetal gene expression of cardiac hypertrophy. Nat Med 4(11):1269-75.

Doenst T, Goodwin GW, Cedars AM, Wang M, Stepkowski S, Taegtmeyer H. 2001. Load-induced changes in vivo alter substrate fluxes and insulin responsiveness of rat heart in vitro. Metabolism 50(9):1083-1090.

Doggrell SA, Brown L. 1998. Rat models of hypertension, cardiac hypertrophy and failure. Cardiovasc Res 39(1):89-105.

Etlinger JD, Goldberg AL. 1977. A soluble ATP-dependent proteolytic system responsible for the degradation of abnormal proteins in reticulocytes. Proc Natl Acad Sci U S A 74(1):54-8.

Fagard R. 2003. Athlete's heart. Heart 89(12):1455-61.

Frey N, Olson EN. 2003. Cardiac hypertrophy: the good, the bad, and the ugly. Annu Rev Physiol 65:45-79.

Glass DJ. 2005. Skeletal muscle hypertrophy and atrophy signaling pathways. Int J Biochem Cell Biol 37(10):1974-84.

Glickman MH, Ciechanover A. 2002. The ubiquitin-proteasome proteolytic pathway: destruction for the sake of construction. Physiol Rev 82(2):373-428.

Goldberg AL. 2005. Nobel committee tags ubiquitin for distinction. Neuron 45(3):339-44.

Goldblatt H, Lynch J, Hanzal RF, Summerville WW. 1934. Studies on Experimental Hypertension : I. The Production of Persistent Elevation of Systolic Blood Pressure by Means of Renal Ischemia. J Exp Med 59(3):347-79.

Goll DE, Neti G, Mares SW, Thompson VF. 2008. Myofibrillar protein turnover: the proteasome and the calpains. J Anim Sci 86(14 Suppl):E19-35.

Goll DE, Thompson VF, Li H, Wei W, Cong J. 2003. The calpain system. Physiol Rev 83(3):731-801.

Grossman W, Jones D, McLaurin LP. 1975. Wall stress and patterns of hypertrophy in the human left ventricle. J Clin Invest 56(1):56-64.

Gustafsson AB, Gottlieb RA. 2008. Recycle or die: the role of autophagy in cardioprotection. J Mol Cell Cardiol 44(4):654-61.

Hamacher-Brady A, Brady NR, Gottlieb RA. 2006. Enhancing macroautophagy protects against ischemia/reperfusion injury in cardiac myocytes. J Biol Chem 281(40):29776-87.

Hill JA, Olson EN. 2008. Cardiac plasticity. N Engl J Med 358(13):1370-80.

Hunter RB, Kandarian SC. 2004. Disruption of either the Nfkb1 or the Bcl3 gene inhibits skeletal muscle atrophy. J Clin Invest 114(10):1504-11.

Iemitsu M, Miyauchi T, Maeda S, Sakai S, Kobayashi T, Fujii N, Miyazaki H, Matsuda M, Yamaguchi I. 2001. Physiological and pathological cardiac hypertrophy induce different molecular phenotypes in the rat. Am J Physiol Regul Integr Comp Physiol 281(6):R2029-36.

Izumo S, Lompre AM, Matsuoka R, Koren G, Schwartz K, Nadal-Ginard B, Mahdavi V. 1987. Myosin heavy chain messenger RNA and protein isoform transitions during cardiac hypertrophy. J Clin Invest 79:970-977.

Izumo S, Nadal-Ginard B, Mahdavi V. 1988. Protooncogene induction and reprogramming of cardiac gene expression produced by pressure overload. Proc Natl Acad Sci USA 85:339-343.

Kassiotis C, Ballal K, Wellnitz K, Vela D, Gong M, Salazar R, Frazier OH, Taegtmeyer H. 2009. Markers of autophagy are downregulated in failing human heart after mechanical unloading. Circulation 120(11 Suppl):S191-7.

Kedar V, McDonough H, Arya R, Li HH, Rockman HA, Patterson C. 2004. Muscle-specific RING finger 1 is a bona fide ubiquitin ligase that degrades cardiac troponin I. Proc Natl Acad Sci U S A 101(52):18135-40.

Kleinman L, Wechsler A, Rembert J, Fedor J, Greenfield J. 1978. A reproducible model of moderate to severe concentric left ventricular hypertrophy. Am J Physiol 234:H515-H519.

Kong SW, Bodyak N, Yue P, Liu Z, Brown J, Izumo S, Kang PM. 2005. Genetic expression profiles during physiological and pathological cardiac hypertrophy and heart failure in rats. Physiol Genomics 21(1):34-42.

Kops GJ, de Ruiter ND, De Vries-Smits AM, Powell DR, Bos JL, Burgering BM. 1999. Direct control of the Forkhead transcription factor AFX by protein kinase B. Nature 398(6728):630-4.

Kurtz TW, Morris RC, Jr. 1987. Biological variability in Wistar-Kyoto rats. Implications for research with the spontaneously hypertensive rat. Hypertension 10(1):127-31.

Latres E, Amini AR, Amini AA, Griffiths J, Martin FJ, Wei Y, Lin HC, Yancopoulos GD, Glass DJ. 2005. Insulin-like growth factor-1 (IGF-1) inversely regulates atrophy-induced genes via the phosphatidylinositol 3-kinase/Akt/mammalian target of rapamycin (PI3K/Akt/mTOR) pathway. J Biol Chem 280(4):2737-44.

Levine B, Kroemer G. 2008. Autophagy in the pathogenesis of disease. Cell 132(1):27-42.

Li XM, Ma YT, Yang YN, Liu F, Chen BD, Han W, Zhang JF, Gao XM. 2009. Downregulation of survival signalling pathways and increased apoptosis in the transition of pressure overload-induced cardiac hypertrophy to heart failure. Clin Exp Pharmacol Physiol 36(11):1054-61.

Li YH, Reddy AK, Ochoa LN, Pham TT, Hartley CJ, Michael LH, Entman ML, Taffet GE. 2003a. Effect of age on peripheral vascular response to transverse aortic banding in mice. J Gerontol A Biol Sci Med Sci 58(10):B895-9.

Li YH, Reddy AK, Taffet GE, Michael LH, Entman ML, Hartley CJ. 2003b. Doppler evaluation of peripheral vascular adaptations to transverse aortic banding in mice. Ultrasound Med Biol 29(9):1281-9.

Li YP, Chen Y, John J, Moylan J, Jin B, Mann DL, Reid MB. 2005. TNF-alpha acts via p38 MAPK to stimulate expression of the ubiquitin ligase atrogin1/MAFbx in skeletal muscle. Faseb J 19(3):362-70.

Matsui Y, Takagi H, Qu X, Abdellatif M, Sakoda H, Asano T, Levine B, Sadoshima J. 2007. Distinct roles of autophagy in the heart during ischemia and reperfusion: roles of AMP-activated protein kinase and Beclin 1 in mediating autophagy. Circ Res 100(6):914-22.

Mearini G, Schlossarek S, Willis MS, Carrier L. 2008. The ubiquitin-proteasome system in cardiac dysfunction. Biochim Biophys Acta 1782(12):749-63.

Meerson FZ. 1969. The myocardium in hyperfunction, hypertrophy and heart failure. Circ Res 25(1):Suppl 2:1-163.

Meier R, Alessi DR, Cron P, Andjelkovic M, Hemmings BA. 1997. Mitogenic activation, phosphorylation, and nuclear translocation of protein kinase Bbeta. J Biol Chem 272(48):30491-7.

Meng L, Mohan R, Kwok BH, Elofsson M, Sin N, Crews CM. 1999. Epoxomicin, a potent and selective proteasome inhibitor, exhibits in vivo antiinflammatory activity. Proc Natl Acad Sci U S A 96(18):10403-8.

Mercadier JJ, Lompre AM, Wisnewsky C, Samuel JL, Bercovici J, Swynghedauw B, Schwartz K. 1981. Myosin isoenzymic changes in several models of rat cardiac hypertrophy. Circ Res 49:525-532.

Milliken MC, Stray-Gundersen J, Peshock RM, Katz J, Mitchell JH. 1988. Left ventricular mass as determined by magnetic resonance imaging in male endurance athletes. Am J Cardiol 62(4):301-5.

Mitch WE, Goldberg AL. 1996. Mechanisms of muscle wasting. The role of the ubiquitin-proteasome pathway. N Engl J Med 335(25):1897-905.

Mizushima N. 2004. Methods for monitoring autophagy. Int J Biochem Cell Biol 36(12):2491-502.

Molkentin JD, Lu JR, Antos CL, Markham B, Richardson J, Robbins J, Grant SR, Olson EN. 1998. A calcineurin-dependent transcriptional pathway for cardiac hypertrophy. Cell 93:215-228.

Morisco C, Sadoshima J, Trimarco B, Arora R, Vatner DE, Vatner SF. 2003. Is treating cardiac hypertrophy salutary or detrimental: the two faces of Janus. Am J Physiol Heart Circ Physiol 284(4):H1043-7.

Opie LH. 2004. Heart physiology: from cell to circulation. Philadelphia: Lippincott Williams & Wilkins. 648 p.

Previlon M, Pezet M, Dachez C, Mercadier JJ, Rouet-Benzineb P. 2010. Sequential alterations in Akt, GSK3beta, and calcineurin signalling in the mouse left ventricle after thoracic aortic constriction. Can J Physiol Pharmacol 88(11):1093-101.

Rajabi M, Kassiotis C, Razeghi P, Taegtmeyer H. 2007. Return to the fetal gene program protects the stressed heart: a strong hypothesis. Heart Fail Rev 12(3-4):331-43.

Raynaud F, Fernandez E, Coulis G, Aubry L, Vignon X, Bleimling N, Gautel M, Benyamin Y, Ouali A. 2005. Calpain 1-titin interactions concentrate calpain 1 in the Z-band edges and in the N2-line region within the skeletal myofibril. Febs J 272(10):2578-90.

Razeghi P, Baskin KK, Sharma S, Young ME, Stepkowski S, Faadiel Essop M, Taegtmeyer H. 2006a. Atrophy, hypertrophy, and hypoxemia induce transcriptional regulators of the ubiquitin proteasome system in the rat heart. Biochem Biophys Res Commun 342(2):361-4.

Razeghi P, Buksinska-Lisik M, Palanichamy N, Stepkowski S, Frazier OH, Taegtmeyer H. 2006b. Transcriptional regulators of ribosomal biogenesis are increased in the unloaded heart. Faseb J 20(8):1090-6.

Razeghi P, Taegtmeyer H. 2005. Cardiac remodeling: UPS lost in transit. Circ Res 97(10):964-6.

Razeghi P, Taegtmeyer H. 2006. Hypertrophy and atrophy of the heart: the other side of remodeling. Ann N Y Acad Sci 1080:110-9.

Reddy AK, Taffet GE, Li YH, Lim SW, Pham TT, Pocius JS, Entman ML, Michael LH, Hartley CJ. 2005. Pulsed Doppler signal processing for use in mice: applications. IEEE Trans Biomed Eng 52(10):1771-83.

Rockman H, Ross R, Harris A, Knowlton K, Steinhelper M, Field L, Ross J, Chien K. 1991. Segregation of atrial-specific and inducible expression of an atrial natriuretic factor transgene in an in vivo murine model of cardiac hypertrophy. Proc Natl Acad Sci USA 88:8277-8281.

Ronnebaum SM, Patterson C. 2010. The FoxO family in cardiac function and dysfunction. Annu Rev Physiol 72:81-94.

Ruivo R, Anne C, Sagne C, Gasnier B. 2009. Molecular and cellular basis of lysosomal transmembrane protein dysfunction. Biochim Biophys Acta 1793(4):636-49.

Satoh M, Minami Y, Takahashi Y, Tabuchi T, Nakamura M. Expression of microRNA-208 is associated with adverse clinical outcomes in human dilated cardiomyopathy. J Card Fail 16(5):404-10.

Schoenheimer R. 1942. The Dynamic State of Body Constituents. Cambridge, MA: Harvard University Press.

Schwartz AL, Ciechanover A. 2009. Targeting proteins for destruction by the ubiquitin system: implications for human pathobiology. Annu Rev Pharmacol Toxicol 49:73-96.

Schwartz K, Boheler KR, de la Bastie D, Lompre AM, Mercadier JJ. 1992. Switches in cardiac muscle gene expression as a result of pressure and volume overload. Am J Physiol 262(3 Pt 2):R364-9.

Schwartz K, de la Bastie D, Bouveret P, Oliviero P, Alonso S, Buckingham M. 1986. α-skeletal muscle actin mRNA's accumulate in hypertrophied adult rat hearts. Circ Res 59:551-555.

Sharma S, Ying J, Razeghi P, Stepkowski S, Taegtmeyer H. 2006. Atrophic remodeling of the transplanted rat heart. Cardiology 105(2):128-36.

Singh RB, Chohan PK, Dhalla NS, Netticadan T. 2004. The sarcoplasmic reticulum proteins are targets for calpain action in the ischemic-reperfused heart. J Mol Cell Cardiol 37(1):101-10.

Skurk C, Izumiya Y, Maatz H, Razeghi P, Shiojima I, Sandri M, Sato K, Zeng L, Schiekofer S, Pimentel D and others. 2005. The FOXO3a transcription factor regulates cardiac myocyte size downstream of AKT signaling. J Biol Chem 280(21):20814-23.

Spirito P, Seidman CE, McKenna WJ, Maron BJ. 1997. The management of hypertrophic cardiomyopathy. N Engl J Med 336(11):775-85.

Strom CC, Aplin M, Ploug T, Christoffersen TE, Langfort J, Viese M, Galbo H, Haunso S, Sheikh SP. 2005. Expression profiling reveals differences in metabolic gene expression between exercise-induced cardiac effects and maladaptive cardiac hypertrophy. Febs J 272(11):2684-95.

Taegtmeyer H, Sen S, Vela D. 2010. Return to the fetal gene program: a suggested metabolic link to gene expression in the heart. Ann N Y Acad Sci 1188:191-8.

Voges D, Zwickl P, Baumeister W. 1999. The 26S proteasome: a molecular machine designed for controlled proteolysis. Annu Rev Biochem 68:1015-68.

Wang X, Su H, Ranek MJ. 2008. Protein quality control and degradation in cardiomyocytes. J Mol Cell Cardiol 45(1):11-27.

Waterlow JC, Garlick PJ, Millward DJ. 1978. Protein turnover in mammalian tissues and in the whole body: Elsevier/North-Holland Biomedical Press. 804 p.

Wildenthal K. 1980. Degradative Processes in Heart and Skeletal Muscle Elsevier Science Ltd 480 p.

Willis MS, Patterson C. 2006. Into the heart: the emerging role of the ubiquitin-proteasome system. J Mol Cell Cardiol 41(4):567-79.

Willis MS, Schisler JC, Portbury AL, Patterson C. 2009. Build it up-Tear it down: protein quality control in the cardiac sarcomere. Cardiovasc Res 81(3):439-48.

Witt SH, Granzier H, Witt CC, Labeit S. 2005. MURF-1 and MURF-2 target a specific subset of myofibrillar proteins redundantly: towards understanding MURF-dependent muscle ubiquitination. J Mol Biol 350(4):713-22.

Wyke SM, Russell ST, Tisdale MJ. 2004. Induction of proteasome expression in skeletal muscle is attenuated by inhibitors of NF-kappaB activation. Br J Cancer 91(9):1742-50.

Young ME, Laws FA, Goodwin GW, Taegtmeyer H. 2001a. Reactivation of peroxisome proliferator-activated receptor alpha is associated with contractile dysfunction in hypertrophied rat heart. J Biol Chem 276(48):44390-5.

Young ME, Razeghi P, Taegtmeyer H. 2001b. Clock genes in the heart: characterization and attenuation with hypertrophy. Circ Res 88(11):1142-1150.

Zhang S, Weinheimer C, Courtois M, Kovacs A, Zhang CE, Cheng AM, Wang Y, Muslin AJ. 2003. The role of the Grb2-p38 MAPK signaling pathway in cardiac hypertrophy and fibrosis. J Clin Invest 111(6):833-41.

Zhao J, Brault JJ, Schild A, Goldberg AL. 2008. Coordinate activation of autophagy and the proteasome pathway by FoxO transcription factor. Autophagy 4(3):378-80.

Zhu H, Tannous P, Johnstone JL, Kong Y, Shelton JM, Richardson JA, Le V, Levine B, Rothermel BA, Hill JA. 2007. Cardiac autophagy is a maladaptive response to hemodynamic stress. J Clin Invest 117(7):1782-93.

VITA

Deborah C. Vela born in Guayaquil, Ecuador on January 1, 1969, the daughter of Maria Cecilia Falquez and Hamilton Raul Vela. She was raised and lived in New York during the 1970s. In 1996, she graduated with a degree of Doctor of Medicine at the Universidad de Guayaquil, in Ecuador. She worked as a general practitioner of medicine in Guayaquil for the next year, before re-emigrating to the United States. Since that time, she has worked in cardiovascular pathology research for the University of Texas Health Science Center at Houston from 2002 to 2005, and later moved on to the Texas Heart Institute at St. Luke's Episcopal Hospital in Houston, Texas. In August 2007 she entered the Graduate School of Biomedical Sciences at the University of Texas Health Science Center, Houston to pursue her Master's of Science degree.